博士学位論文

Nonlinear Fluorescence Probes: Development and Application to Super-Resolution Microscopy

望月健太郎

2014 年 12 月

大阪大学大学院工学研究科

Contents

Introduction

The word of "nano" has been such familiar that it is used even in TV commercials or as the product name for daily items nowadays. This must be largely owing to the common use of the "nano" as a scale of length or size unit in the recent science and technology. In the area of optics, which is my major, the word of "optical nanoscopy" has often been seen recently instead of "optical microscopy" [1-3]. Optical microscopy is one of the strategies developed to observe materials with the magnified scale by the use of light. Although its spatial resolution had been limited to sub-micrometer due to the diffraction property of light [4], the recent advances realized break of the limit by developing super-resolution microscopies. The advances have been especially marked in fluorescence microscopy, and a part of the achievements was honored with the Novel Prize in Chemistry in 2014. Nowadays, the use of these developed microscopies enables us to visualize the distribution and even dynamics of single molecules such as a protein in a living cell.

The recent developments of the super-resolution fluorescence microscopies have been realized by manipulating the optical response of fluorescent molecules. In the fluorescence microscopy, fluorescent molecules tagged on targets are excited by light irradiation, and fluorescence emitted from them is detected to construct microscopic images of the targets [5,6]. The spatial resolution of conventional fluorescence microscopies had been determined with the diffraction limit of the incident light or fluorescence. Stimulated emission depletion (STED) microscopy realizes the super spatial resolution by utilizing the nonlinear optical response of fluorescent molecules caused by saturation effects [7,8]. Localization microscopy harnesses the fluorescence switching of proteins/dyes, achieving resolutions of a few nanometers with biological samples [9-11]. Aside from these techniques, two-photon excitation microscopy (TPEM) also realizes the spatial resolution beyond the diffraction limit by using nonlinear fluorescence response of fluorescent molecules [12,13]. TPEM is performed with a laser-scanning microscope without complex excitation process and computational post-processing. However, it has not been recognized as a super-resolution imaging technique. The reason why TPEM has not been recognized as

super-resolution microscopy is because of the use of near infrared light as excitation source, which provides a lower spatial resolution than visible light even through the nonlinear effect can improve the spatial resolution. In my doctoral research, I aimed the realization of nonlinear fluorescence responses using visible light excitation in order to achieve super-resolution imaging just with a laser-scanning microscope. To realize this aim, fluorescent probes providing stepwise multi-photon excitation were developed.

In chapter 1 in this dissertation, the spatial resolution limit in fluorescence microscopy due to the diffraction property of light is explained. For the improvement of this resolution limit, two approaches have been accomplished by researchers, where one is based on the spatial filtering and the other is based on the manipulation of optical response of fluorescent molecules. As a typical technique realized by the modification of optical setups, confocal laser-scanning microscopy is introduced, and then recent advances of super-resolution microscopy which have been mainly realized by the manipulation of fluorescent molecules are reviewed.

In chapter 2, the fundamentals of TPEM are explained. The mechanism of spatial resolution improvement by two-photon excitation of fluorescent molecules is described, and the spatial resolution limit in practical uses of TPEM is introduced, which is derived from the use of near-infrared light as excitation source.

In chapter 3, the realization of stepwise two-photon excitation with visible-wavelength CW light by the use of photoinduced charge separation (PCS) is shown. A fluorescent probe with two electron donors and one electron acceptor (nitro-bisBODIPY) is designed. The realization of the stepwise two-photon excitation by using this probe is confirmed by the measurement of fluorescence response and fluorescence imaging using the probe.

In chapter 4, the photophysical mechanism of the nonlinear fluorescence response via PCS is investigated by building a photophysical model of nitro-bisBODIPY. According to the model, the simulation of fluorescence response of the probe is conducted, and compared with the experimental results to evaluate accuracy of the model.

In chapter 5, a concept to achieve nonlinear fluorescence response with utilizing spirocycle opening is shown. In this scheme, the stepwise three-photon excitation is

realized via two-photon absorption to induce the spirocycle opening and subsequent one-photon absorption under visible-wavelength pulsed excitation to excite the fluorescence. The realization of the stepwise three-photon excitation is confirmed with the detection of fluorescence response of the spirocyclic compounds.

In chapter 6, the concept based on the development of probes is applied to Raman microscopy for cells. A probe to achieve high-resolution Raman microscopy is fabricated inside cells by laser-induced photoreduction. The probe composed of gold nanoparticles (NPs) is fabricated at desired positions in cells. The detection of SERS spectra using the probe inside cells is conducted and the practical utility of this technique is investigated.

References

[1] J. Fölling, V. Belov, R. Kunetsky, R. Medda, A. Schönle, A. Egner, C. Eggeling, M. Bossi, and S. W. Hell, *Angew. Chem. Int. Ed.* **46**, 6266-6270 (2007)

[2] I. Testa, N. T. Urban, S. Jakobs, C. Eggeling, K. I. Willig, and S. W. Hell, *Neuron* **75**, 992-1000 (2012)

[3] A. Diaspro, *"NANOSCOPY AND MULTIDEMENSIONAL OPTICAL FLUORESCENCE MICROSCOPY"* Taylor and Francis Group (2010)

[4] M. Born and E. Wolf, "Principles of Optics" PERGAMON PRESS (1980)

[5] 御橋廣眞　編「蛍光分光とイメージングの手法」日本分光学会 (2006)

[6] J. R. Lakowicz, "Principles of Fluorescence Spectroscopy" Springer (2006)

[7] S. W. Hell and J. Wichmann, *Opt. Lett.* **19**, 780-781 (1994)

[8] T. A. Klar and S. W. Hell, *Opt. Lett.* **24**, 954-956 (1999)

[9] M. J. Rust, M. Bates, and X. Zhuang, *Nat. Methods* **3**, 793-795 (2006)

[10] E. Betzig, G. H. Patterson, R. Sougrat, O. W. Lindwasser, S. Olenych, J. S. Bonifacino, M. W. Davidson, J. Lippincott-Schwartz, H. F. Hess, *Science* **313**, 1642-1645 (2006)

[11] S. T. Hess, T. P. K. Girirajan, and M. D. Mason, *Biophys. J.* **91**, 4258-4272 (2006)

[12] W. Denk, J. H. Strickler, W. W. Webb, *Science* **248**, 73-76 (1990)

[13] A. Diaspro, *"Confocal and Two-Photon Microscopy"* Wiley-Liss (2002)

Chapter 1: Review of super-resolution fluorescence microscopy

Introduction

To achieve the spatial resolution beyond the limit determined with the diffraction property of light, various techniques have been developed. These advances were especially marked in fluorescence microscopy. In this chapter, the limit of spatial resolution in optical microscopy is discussed, and a super-resolution technique "confocal microscopy" realized by the modification of optical setups is introduced. Subsequently recent great advances in the development of super-resolution fluorescence microscopy is reviewed, which has been performed by the manipulation of optical response of fluorescent molecules.

1.1 Resolution limit in fluorescence microscopy

Typical optical microscopy including fluorescence microscopy has the limit of spatial resolution due to the diffraction limit of the light. Tracing the history of the optical microscopy, the zoom of a view by the combination of lenses was discovered by Hans Jansen and Sacharias Jansen in 1550s, who were the Dutch glass polishers [1]. In the 17th century, “the simple optical microscope” was developed by Antonie van Leeuwenhoek, and the spatial resolution of 1 μm was achieved. This microscopy had been used for the observation of biological samples for the first time and the existence of microorganisms was found in this time. The microscopy which can be mentioned as the base of current optical microscopies was established by Robert Hooke as “the compound optical microscope”, which didn’t require considerable skills to be used. After that, various kinds of optical microscopies had been established, basically in order to acquire higher spatial resolution. In 1903, dark field microscopy was invented and contributed to clarify the property of colloidal solution, which achievement was honored as the Novel Prize in Chemistry in 1925. In 1930, differential polarization microscopy was developed and the sterical optical imaging of samples with high resolution was accomplished. Phase-contrast microscopy was established in 1935 and the optical imaging of transparent specimens even

in aqueous solutions was performed. This invention was honored as the Novel Prize in Physics in 1953. Then, fluorescence microscopy was invented in the early 1990s and has been advanced along with the development of fluorescence antibody technique. In fluorescence microscopy, fluorescence dyes or proteins are tagged on targets and the distribution or structures of targets are visualized by detecting fluorescence signals from them. Same as the microscopies mentioned above, this method realizes the imaging of transparent samples such as biological cells with the high spatial resolution. Additionally, the observation target can be selected by the staining way of the choice of fluorescent probes. This property was applied to observe multiple targets even in a same specimen. Furthermore, since the fluorescence intensity changes temporally and depends on the environmental condition, we can obtain not only the spatial distribution of targets but also the environmental information of them quantitatively. While these microscopies had been established, however, the limitation of the spatial resolution in the optical microscopy had been gradually uncovered. Ernst Abbe established the theory for this limitation using the concept of numerical aperture (NA) of the lens in 1976. In his theory, it was shown that light of a wavelength λ focused by a lens is impossible to distinguish objects located closer than distance $d = \lambda / (2NA)$ in the coherent illumination [2,3]. This is derived from the fact that a single point is imaged as a blurred spot when it is observed with lens-based optical microscopy because of the diffraction property of light, and this spread image is expressed as “point spread function (PSF)”. Therefore, the observation of objects which are closely located each other results to the detection of overlapped image. In fluorescence microscopy, the minimum resolvable distance in lateral plane was defined with the Rayleigh criterion [4]. In the Rayleigh criterion, the spatial resolution is described as the distance between the positions of the first minimum and central maximum in intensity distribution. To quantify resolution, the Rayleigh criterion corresponds to the separation at which a 26.4 % contrast is acquired [5]. Under an ideal optical condition, the lateral distance of two point objects by the 26 % criterion is almost equivalent to the Rayleigh criterion. This allows us to define the lateral resolution for a conventional fluorescence microscope as the distance between the first minimum and central maximum. This distance

is given by,

$$d = 1.22\,\lambda / 2NA = 0.61\lambda / NA \qquad (1\text{-}1)$$

In practice, it is troublesome to detect the location of an intensity minimum, hence to measure the full-width half-maximum (FWHM) of the PSF of a point object is common to determine the resolution experimentally.

From the equations in both Abbe's theory and Rayleigh criterion, it is indicated that the spatial resolution is limited with NA of a lens and wavelength of light. In order to break this limit, various techniques had been developed by improving optical setups especially based on fluorescence microscopy [6-8]. Confocal microscopy is one of the techniques to achieve super spatial resolution beyond the diffraction limit of light, and the technique nowadays becomes one of the essential tools in the imaging research due to its simple optical setup and various advantages other than the improvement of spatial resolution [6,9]. Also in my doctoral research, confocal microscopy was used as the basic optical setup.

1.2 Confocal microscopy for resolution improvement

Confocal microscopy is one of super-resolution microscopies achieved by the modification of optical setup. It was first proposed and established by M. Minsky in 1961 and had been advanced mainly by T. Wilson and C. Sheppard [5,6]. The advantage of confocal microscopy is represented by the acquisition of resolution ability also along the optical axis in the imaging [10]. In other words, confocal microscopy performs optical sectioning capability. Besides this optical sectioning ability, confocal microscopy realizes spatial resolution beyond the diffraction limit of light in focal plane. Confocal microscopy is based on laser scanning illumination. Laser light is focused on objects by an objective lens, and scanned across objects point-by-point. When the objects are fluorescent molecules, emitted fluorescence signals from the laser-focused point are collected with the objective lens and detected by a photodetector. Finally, images are constructed according to the detected signal intensities from each point. The name of confocal microscopy is derived

from the existence of a confocal pinhole in front of the detector, and this makes the difference between confocal and non-confocal microscopy even if both of them are based on laser-scanning illumination. The confocal pinhole works to detect only signals from in-focus of a laser spot but not from out-focus, thereby suppressing background signals form out-focus plane. This property shows a great advantage in observing thick three-dimensional samples.

1.3 Manipulation of molecular response for resolution improvement

The limit of spatial resolution determined with the optical setup was broken by manipulating emission properties of fluorescent molecules. In the aspect of a focal plane resolution achieved by the improvement of optical setup, the resolution in the confocal microscopy can be described as its limit. In other words, more upgrade of optical setups to improve the spatial resolution has not been expected. Then the key to improve the resolution was found in the manipulation of molecular response of fluorescent molecules. Here I'd like to review the super-resolution fluorescence microscopies including STED microscopy which promoted many other kinds of super-resolution microscopy.

STED microscopy

STED (Stimulated emission depletion) microscopy was proposed by S. Hell in 1994 and verified by his research group in 1999 with a resolution improvement from ~150 nm to ~100 nm under 388 nm excitation [11,12]. In STED microscopy, a doughnut-shaped light (STED beam) is irradiated on a focused excitation light to suppress fluorescence emission by inducing stimulated emission. Stimulated emission is one of radiative relaxation pathways of excited molecules, other than fluorescence emission. Fluorescent molecules distributed in the area irradiated with the STED beam relax their energy by the stimulated emission although they are excited by the excitation light. Accordingly, only the fluorescent molecules in the center of the excitation light where is the inside of the doughnut-shaped STED beam is permitted

to emit fluorescence. Therefore, the improvement of the spatial resolution is given. The improvement degree of the spatial resolution is determined by the minimized hole size of the STED beam. To minimize the hole size, nonlinear relationship between the stimulated emission intensity and the STED beam intensity is utilized. The nonlinear relation ship is attributed to the saturation of the stimulated emission induced by the irradiation of the high intensity STED beam. In recent progresses, a few nanometer of spatial resolution was achieved for a fluorescence imaging of nanodiamonds with STED microscopy, and a few dozen nanometer for biological samples [13].

SAX microscopy

SAX (Saturated excitation) microscopy also realized super spatial resolution by the use of nonlinear optical response of fluorescent molecules [14,15]. In SAX microscopy, the nonlinear optical response is find out in the saturation effect of fluorescence emission of fluorescent molecules via the irradiation of high intensity excitation light. Since the energy transition in relaxation process of excited molecules has a lifetime, the linear relationship in the cycle of excitation and relaxation process is collapsed by the intensity higher than a constant value. In the scanning of excitation light for the distribution of fluorescent molecules, the modulation of excitation intensity with a specific frequency is run. As results, the fluorescence response is detected which intensity follows the modulated intensity of the excitation light. Because of the nonlinear relationship via the saturation effect, however, the fluorescence response against the high intensity excitation is distorted. This distorted response can be dissolved to the combination of a fundamental wave and high frequency waves which frequency is integral multiple of that of the fundamental wave. And since the integral-multiplied waves are generated only at the center of the focused excitation light where the intensity is higher, the resolution improvement is accomplished by extracting only those waves in the imaging. The improvement degree is determined with the selection of the integral multiple of those high frequency waves. The nonlinear fluorescence response of fluorescent molecules by the saturation effect is utilized in structured illumination microscopy, and the super resolution of <100 nm was achieved

[16].

Localization microscopy

Localization microscopy mainly known as PALM/STORM is one of super-resolution microscopy, which realizes quite high spatial resolution [17-19]. In the localization microscopy, a few nanometer spatial resolution was achieved even for fluorescence imaging of biological samples. This technique was produced as the result of development of the single-molecule imaging. By the recent progress of single-molecule imaging technique, the coordinate of a fluorescence molecule can be limited within the accuracy of a few nanometer by the mathematical calculation although its fluorescence signal were detected as a intensity distribution described by the diffraction limit. In the localization microscopy, this single-molecule imaging was treated for individual fluorescent molecules distributed in samples through the molecular switching of fluorescent condition of the molecules. The fluorescent images of individual molecules are finally accumulated, and thereby the fluorescence image of the distribution of the molecules can be constructed. The molecular switching of fluorescent molecules, which is another key in localization microscopy, is based on the photochromism. Photochromism is defined as the change of optical properties induced by the interaction with the irradiated light, and especially it describes the change of fluorescent condition of molecules, here. Although the photochromism of fluorescent molecules has been known and research for a long time, recent advances achieved us to prepare various fluorescent molecules with the property of photochromism or fluorescence switching, including organic fluorescent dyes and fluorescent proteins.

The first localization microscopies are known as photoactivated localization microscopy (PALM) by E. Betzig et al., fluorescence photoactivated localization microscopy (fPALM) by S. T. Hess et al. and stochastic optical reconstruction microscopy (STORM) by M. J. Rust, all of them were reported in 2006. The shortcomings behinds the super spatial resolution such as low temporal resolution, the limited condition of samples, high excitation intensity have been improved by upgrading light-irradiation or

fluorescence-detection schemes or using different mechanism of molecular switching [20].

RESOLFT

The use of molecular switching was accomplished to develop Reversible Saturable Optical Fluorescence Transitions (RESOLFT) microscopy, which was proposed in 2003 and verified in 2005 by the research group of S. Hell [21,22]. The system of RESOLFT microscopy is based on STED microscopy in terms of the resolution improvement via the suppression of fluorescence emission from the excitation area other than the center part. In RESOLFT microscopy, the suppression of fluorescence emission of molecules is performed via the molecular switching instead of the stimulated emission in STED microscopy.

References

[1] 野島博　編「顕微鏡の使い方ノート 第２版」羊土社 (2006)

[2] M. Born and E. Wolf, *"Principles of Optics"* Pergamon Press (1980)

[3] S. W. Hell, *Nat. Methods* **6**, 24-32 (2009)

[4] 御橋廣眞 編 「蛍光分光とイメージングの手法」日本分光学会 (2006)

[5] A. Diaspro, *"Cofocal and Two-Photon Microsocpy"* Wiley-Liss (2002)

[6] T. Wilson and C. Sheppard, *"THEORY AND PRACTICE OF SCANNING OPTICAL MICROSCOPY"* Academic Press (1984)

[7] S. Hell and E. H. K. Stelzer, *Opt. Comm.* **93**, 277-282 (1992)

[8] M. G. L. Gustafsson, *J. Microscopy* **198**, 82-87 (2000)

[9] T. R. Corle and G. S. Kino, *"Confocal Scanning Optical Microscopy and Related Imaging Systems"* Academic Press (1996)

[10] 河田聡　編「超解像の光学」日本分光学会 (1999)

[11] S. W. Hell and J. Wichmann, *Opt. Lett.* **19**, 780-782 (1994)

[12] T. A. Klar and S. W. Hell, *Opt. Lett*. **24**, 954-956 (1999)

[13] N. T. Urban, K. I. Willig, S. W. Hell, and U. V. Nagerl, *Biophys. J.* **101**, 1277-1284

(2011)

[14] K. Fujita, M. Kobayashi, S. Kawano, M. Yamanaka, and S. Kawata, *Phys. Rev. Lett.* **99**, 228105 (2007)

[15] M. Yamanaka, Y. Yonemaru, S. Kawano, K. Uegaki, N. I. Smith, S. Kawata, K. Fujita, *J. Biomed. Opt.* **18**, 126002 (2013)

[16] R. Heintzmann and T. M. Jovin, *J. Opt. Soc. Am. A* **19**, 1599-1609 (2002)

[17] M. J. Rust, M. Bates, and X. Zhuang, *Nat. Methods* **3**, 793-795 (2006)

[18] E. Betzig, G. H. Patterson, R. Sougrat, O. W. Lindwasser, S. Olenych, J. S. Bonifacino, M. W. Davidson, J. Lippincott-Schwartz, H. F. Hess, *Science* **313**, 1642-1645 (2006)

[19] S. T. Hess, T. P. K. Girirajan, and M. D. Mason, *Biophys. J.* **91**, 4258-4272 (2006)

[20] B. Huang, W. Wang, M. Bates, and X. Zhuang, *Science* **319**, 810-813 (2008)

[21] S. W. Hell, S. Fakobs, and L. Kastrup, *Appl. Phys. A* **77**, 859-860 (2003)

[22] M. Hofmann, C. Eggeling, S. Jakobs, and S. W. Hell, *Proc. Nat. Am. Soc.* **102**, 17565-18569 (2005)

Chapter 2: Two-photon excitation microscopy (TPEM)

Introduction

As the technique to achieve a spatial resolution beyond the diffraction limit, two-photon excitation microscopy (TPEM) is also known besides super-resolution microscopies introduced in chapter 1. TPEM is realized just with the use of a laser-scanning microscope and without the complicated excitation way or computational post-processing. However, TPEM has not been recognized as the super-resolution microscopy. In this chapter, the system of TPEM and the mechanism of resolution improvement are introduced firstly. Then the limitation of the resolution improvement in practical use of TPEM is explained.

2.1 Fundamentals of electronic transition

Two-photon excitation of a fluorescent molecule is accomplished by the step that the molecule simultaneously absorbs two incident photons and emit one fluorescence photon [1]. Fluorescence emission is one of relaxation processes of electronic-excited molecules. Molecules are electronically excited with several triggers, and photon absorption is one of them. These molecular phenomena based on the electronic transition can be assumed to occur in the static framework of atomic cores. To understand the details in two-photon excitation, we need firstly consider the fundamentals of electronic transition including photon absorption, fluorescence emission by molecules.

The energy of a molecule is transited to the higher state by electronic transition [2]. The energy difference between the excited state and ground state of a molecule is described as,

$$h\nu = E_1 - E_0 \qquad (2\text{-}1)$$

, where h and ν denote the Planck constant and the frequency of incident light. Three phenomena contributing the electron transition in molecules were identified by Einstein, which are stimulated absorption, stimulated emission, and spontaneous emission [3].

Stimulated absorption is the molecular electronic transition from the low energy state to the high energy state, that is triggered by light irradiation. Stimulated emission is the transition form the high energy state to low energy state triggered by the interaction with incident light, resulting to the emission of a photon (frequency: ν). And spontaneous emission is photon emission as a result of spontaneous electron transition from the high to low energy state, which is known as fluorescence emission. Einstein identified that the rate of this spontaneous emission is independent on intensity of the incidence light. After light absorption, the energy level of the molecule transits nonradiatively from the initial vibrational state to the lowest vibrational state in the excited electronic state, triggered by collisions with the surrounding molecules. To recover to the ground electronic state, however, it is necessary to dissipate large energy. Therefore, the excited molecules take long time to be relaxed via spontaneous emission. It is known that excitation of a fluorescent molecule happens within ~ 10^{-15} s, the fluorescence lifetime is ~ 10^{-9} s, internal conversion that is one of nonradiative decay from the high energy state to the low energy state happens within ~ 10^{-12} s [4,5].

Fluorescence lifetime can be explained as a time constant for the molecule to spend for the transition from the excited to the ground singlet state. Using rate constants for fluorescence emission k_{em} and non-radiative decay k_{nr}, fluorescence lifetime τ is described as,

$$\tau = 1/(k_{em} + k_{nr}) \qquad (2\text{-}2)$$

Originally, the fluorescence time was defined as a time until fluorescence intensity decreases to 1/e of the initial intensity as expressed by the following equation.

$$I = I_0 \exp(-t/\tau) \qquad (2\text{-}3)$$

This indicates that 63 % of fluorescent molecules return to their ground state at $t = \tau$. The characteristic of a fluorescent molecule is often evaluated also by quantum yield (QE) for

fluorescence emission, aside from fluorescence lifetime. QE is the number of fluorescence photons against the number of photons the molecule absorbs. When the rate constant of fluorescence emission and other relaxation process including non-radiative decay as k_{em} and k_{other}, QE is given by,

$$\Phi = k_{em}/(k_{em} + k_{other}) \qquad (2\text{-}4)$$

For now, the electronic transitions of fluorescent molecules were assumed to be started only with the single photon absorption. By the irradiation of intense laser such as ultra-short pulsed laser light, fluorescent molecules can be excited by simultaneous absorption of two or more photons. The theory of this two-photon excitation was established by Mayer in 1931 [6]. The experimental investigation of this phenomenon was conducted after the laser was invented. Soon after that, the two-photon excitation technique was applied to biological and medicine researches [7].

2.2 Nonlinear fluorescence response by two-photon excitation

By the two-photon excitation, fluorescent molecules show 2nd order nonlinear fluorescence response. This nonlinearity by two-photon excitation induces the distortion of fluorescence PSF against the excitation PSF, resulting to the improvement of spatial resolution in TPEM. The two-photon excitation is induced by two longer-wavelength photons which simultaneously arrive to a fluorescent molecule, following which a single fluorescence photon is emitted. In this two-photon excitation and fluorescence emission process, one photon is generated as fluorescence by exploiting two incident photons. Thus, the two-photon excited fluorescence intensity is proportional to the square of the excitation intensity. What is important is that this process is induced only in the laser focus. To induce two-photon excitation, it is necessary for two photons to arrive at a fluorescent molecule in the same quantum event, which temporal window is to 10^{-16} s [8]. This condition is satisfied under extremely intense excitation intensity such as femtosecond pulse laser excitation.

2.3 Resolution limit in TPEM

TPEM has not been recognized as a super resolution technique because of the general use of near-infrared light source [9]. The developed fluorescent molecules have their absorption bands in visible-wavelength range. Therefore, the excitation wavelength for two-photon excitation is limited to the near-infrared wavelength, which is around double of the visible wavelengths. In addition, the use of near-infrared wavelength for the two-photon excitation has been accelerated because it allows us to observe deep tissue structures due to the lower absorbance of near-infrared light in tissue samples than that of visible light. As explained in chapter 1, the use of near-infrared light provides lower spatial resolution than the use of visible light even though the nonlinear effect can improve the spatial resolution.

References

[1] J. R. Lakowicz, *"Principles of fluorescence spectroscopy"* Springer (2006)

[2] P. W. Milonni and J. H. Eberly, *"LASERS"* John Wiley & Sons (1988)

[3] P. Atkins and J. de Paula, *"ATKINS' physical chemistry"* OXFORD (2006)

[4] 御橋廣眞　編「蛍光分光とイメージングの手法」日本分光学会 (2006)

[5] C. Eggeling, A. Vokmer, and C. A. M. Seidal, *Chem. Phys. Chem.* **6**, 791-804 (2005)

[6] M. Goppert-Mayer, *Ann. Phys.* **9**, 273-295 (1931)

[7] W. Denk, J. H. Strickler, W. W. Webb, *Science* **248**, 73-76 (1990)

[8] A. Diaspro, *"Cofocal and Two-Photon Microsocpy"* Wiley-Liss (2002)

[9] F. Helmchen and W. Denk, *Nat. Methods*, **2**, 932-940 (2005)

Chapter 3: Nonlinear fluorescence response via photo-induced charge separation (PCS)

Introduction

As first trial to achieve the nonlinear fluorescence response with visible CW light excitation, I propose the use of photoinduced charge separation (PCS) [1]. In my proposition, a probe composed of two fluorescent molecules and one electron acceptor is expected to provide stepwise two-photon excitation by the visible-wavelength CW light irradiation. PCS is induced intramolecularly and used as the initiating reaction to switch ON/OFF of fluorescence emission of probes.

3.1 PCS

In this section, it is explained that the quenching of fluorescence of fluorescent molecules can be realized via PCS between a fluorescent molecule and an electron acceptor. The minimum structural unit of materials can be assumed as an atom. Around an atom, electrons exist with their specific orbital. Through the bounding of atoms, their electron orbital also generates complex bounding orbital [2]. A molecule has specific electron orbital and this makes the bias in the distribution and density of electrons around the molecule. As results of this bias, some molecules have electronic properties such as electron donating ability or electron acceptability. When a molecule with electron donating ability and a molecule with electron acceptability physically close to each other, a electron of the molecule with electron donating ability has a potential to transfer into the electron orbital of the molecule with electron acceptability [3]. Here, a fluorescent molecule can be the electron donor. In this situation, the excited energy of the fluorescent molecule which was supposed to relax with radiative/nonradiative relaxation is dissipated by the generation of charge-separated state through electron transfer to the electron acceptor. Accordingly, the electron transfer or the charge separation realizes the quenching of fluorescence emission. In detail, the non-working of electron acceptor permits the fluorescence emission

of the fluorescent molecule while the working of the acceptor prohibits that, resulting to the control of ON/OFF of fluorescence emission of the molecule. In order to give the basic about charge separation, the electron donating ability and acceptability can be explained from the aspect of thermal mechanism, and then some examples of the charge separation between the electron donor and acceptor is shown. Here, it is assumed that the electron transfer occurs after a molecule settles in equilibrium condition but not in the Frank-Condon condition.

In general, the electron donating ability and acceptability rises in the excited states of atoms/molecules. This can be explained in terms of ionization potential (IP). IP is defined as the energy needed to transfer a bounded electron to infinity when an atom or molecule donates it. In short, IP is described as the subtraction of the orbital energy at infinity from the atom/molecule and that of innermost orbital.

$$IP = E_{\infty} - E_1 = 0 - (-13.6 \text{ (Hydrogen)}) = 13.6 \text{ eV} \qquad (3\text{-}1)$$

In other words, an electron to be transferred exists more inner of a molecule, thus the molecule is ionized easily due to its small IP. Second is the case about the energy required for an electron to be accepted into a lowest unoccupied molecular orbital (LUMO) from an orbital at infinity. Because of the attraction force between an electron and a nuclear, an energy is release in the electron acceptance. The energy released in the electron acceptance from an orbital at infinity to an orbital (energy: E) can be described as -IP, which is the reverse-signed IP of anion. This reverse-signed IP can be donated as electron affinity (EA), which has a positive sign and means an exothermal reaction. When an electron acceptor is excited, EA is higher than that of electron acceptor in the ground state due to a generation of a hole in lowest orbital.

$$A + e^- \rightarrow A^- - IP \qquad (3\text{-}2)$$

$$A^* + e^- \rightarrow A^- - IP' \qquad (3\text{-}3)$$

$IP' = IP + E_{00}$ (3-4)

Accordingly, the energy between an electron donor and an acceptor in electron transfer is described as,

$D + A \rightarrow D^+ + A^-$ (3-5)

$\Delta E = IP - EA$ (3-6)

When the donor is excited,

$D^* + A \rightarrow D^+ + A^-$ (3-7)

$\Delta E = IP - EA - E_{00}$ (3-8)

This is also applied when the acceptor is excited. Based on the aspects mentioned above, I'd like to show some examples of molecules providing electron donating ability or acceptability. Amines are known to bear low IP and show high electron donating ability. The IP of amines is equivalent to the energy to ionize one of non-covalent **n** electron. Non-covalent electron is easy to be withdrawn by electron acceptors because they are not involved in the atomic bond. Therefore, molecules with non-covalent electrons including amines are known as strong electron donors. Naphthalene and anthracene have small IP, but this is because **π** electrons in these kinds of organic hydrocarbon are easy to be withdrawn. Excitation of these molecules with **π** electrons increases its electron donating ability because **π*** orbital has relatively high energy. And distorted ring-shaped molecules also show strong donating ability. This is attributed to the high energy of **σ** orbital in these structures. Inversely, cyano aromatic compounds show electron acceptability because of low electron density in **π** orbital by the strong electron withdrawing of cyano group. The

EA of 1-cyano naphtalene is higher than that of naphtalene. In the **π-π*** excited state of cyano aromatic compounds, furthermore, higher electron acceptability is borne due to the generation of electron hole in π orbital which energy is low. Quinone and carbonyl compounds also show strong electron acceptability because of the same reason.

The probability of electron transfer between a fluorescent molecule and an electron acceptor depends not only on the rule in thermal dynamics but also on the lifetime of excited state of the fluorescent molecule. The rate constant of electron transfer k_{et} can be estimated by the fluorescence lifetime over the concentration change of the electron acceptor. This method is based on the Stern-Volmer equation as shown below.

$$1/\tau_{Fl} - 1/\tau'_{Fl} = k_{ET}[Q] \qquad (3\text{-}9)$$

Here, τ_{Fl} and τ'_{Fl} denote fluorescence lifetimes of the fluorescence molecule under the existence and absence of the acceptor, respectively. Based on the equation, k_{ET} can be required as the slope of a function between $1/\tau_{Fl}$ and [Q]. And a quantum yield of electron transfer φ_{ET} is defined as below [4].

$$\varphi_{ET} = k_{ET} / (k_{ET} + k_{Fl} + k_{Other}) \qquad (3\text{-}10)$$

The lifetime of a charge-separated state or a charge-separated pair τ_{CS} is described using the rate constant of electron recombination (k_{ER}) as the following [5].

$$\tau_{CS} = 1 / k_{ER} \qquad (3\text{-}11)$$

The lifetime of a charge-separated state strongly depends on the coulomb interaction and the polarity of solvents.

For now, PCS was described assuming to occur intermolecularly and intramolecularly. Here the differences between intermolecular and intramolecular PCS are explained. Atoms or molecules keep rapid reaction in the quite short time in the chemical reaction. This

dynamic behavior includes the change of positional relationship and orientation between ions, and conformation. Especially the intramolecular charge separation is known as the complicated phenomenon. The intramolecular charge separation occurs through the space or the linker molecules. The charge separation through the space preferentially occurs when molecules have the overlap between orbitals of a donor and acceptor. The probability is determined based on the volume of the overlap. Accordingly, the rate constant of electron transfer increases with the volume of the overlap of orbitals. On the other hand, the charge separation through the linkers occurs in the molecule in which a donor and an acceptor are separated sufficiently. This type of electron transfer depends on the property and number of the linker molecules. An electron of the donor moves to LUMO of the acceptor through LUMO of linker molecules, or a positive hole in HOMO of the acceptor moves to an occupied orbital of the donor.

3.2 Stepwise two-photon excitation

Here I'd like to explain about my concept for nonlinear fluorescence response utilizing PCS. As mentioned above, the pair of a fluorescence molecule (electron donor) and an electron acceptor shows fluorescence quenching via PCS. I propose a fluorescent probe consisting of two fluorescent molecules and one electron acceptor. When one of these two donors is excited by an incident photon, a charge-separated state is formed via PCS between the donor and the acceptor without emitting a fluorescence photon. In this condition, the probe is still capable of absorbing one more incident photon through the other donor and emitting fluorescence if it is assumed that only one donor can form the charge-separated state with the acceptor.

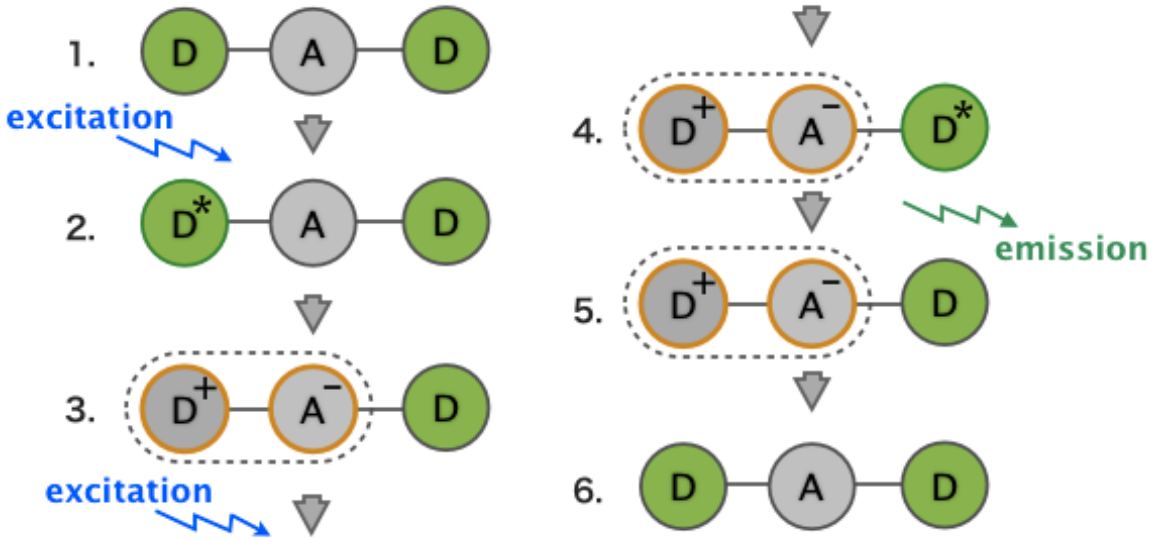

Fig. 3-1. Proposed scheme of the nonlinear fluorescence emission via molecular switching by PCS. D and A denote an electron donor and an electron acceptor, respectively. The symbols of *, + and − represent an excited state, a positive charge, and a negative charge, respectively. (Reprinted with permission from Mochizuki, K. et al., Jpn. J. Appl. Phys. (In press). Copyright 2015 by the Japan Society of Applied Physics.)

Since the probe requires the interaction with two photons to emit fluorescence, the nonlinear relationship between excitation and fluorescence is expected. Then the fluorescence intensity is not linearly proportional to the excitation light intensity, and consequently, the point-spread-function (PSF) of the fluorescence emission becomes smaller than that in a single-photon excitation. Therefore, the spatial resolution can be improved by using the proposed fluorescent probe in a conventional laser scanning microscope. Some similar ideas for inducing nonlinear fluorescence response have been proposed by using fluorescence resonance energy transfer (FRET) [6-9] and bright-dark state switching of dyes [10], but no experimental results achieving resolution improvement only with a confocal microscope and single excitation wavelength have been reported in my understand. It is noteworthy that the quantum yield of fluorescence quenching is required to be high enough, otherwise linear fluorescence response via one-photon

excitation process covers the nonlinear fluorescence response. Under utilizing FRET, the simulation results of fluorescence response showed that the more than 90 % quantum yield of FRET is needed to detect the nonlinear fluorescence response [6]. It is predicted that similar value of quantum yield is required for PCS in my concept.

3.3 Synthesis of a nonlinear fluorescence probe

To demonstrate my concept, a compound was synthesized. The compound consists of two boron-dipyrromethene (BODIPY) and one nitro-benzene, according to the structure of two electron donors and one electron acceptor [D-A-D], and was named nitro-bisBODIPY. BODIPY is a novel fluorescent dye which is commercially available. It has attractive features such as high photostability and high molar absorption coefficient (80,000 $M^{-1}cm^{-1}$), high fluorescence quantum yield in various solvents, and those properties can be tuned by chemical modifications [11-14]. Therefore, it has been introduced as replacements for conventional well-used fluorescent labels such as fluorescein or rhodamines [5]. Nitro-benzene is famous as a strong electron acceptor because of its low LUMO energy [15,16]. Nitro groups make benzene electron-deficient by its strong electron-acceptability effect, and lower the LUMO energy of benzene. BODIPY and nitro-benzene were placed orthogonally each other to prevent the share of LUMO and HOMO of them as shown in Fig. 3-3.

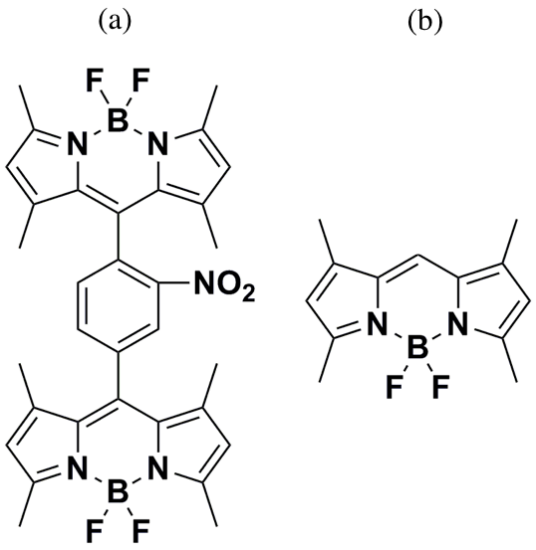

Fig. 3-2. The chemical structure of (a)nitro-bisBODIPY, (b)BODIPY (505/515). (Reprinted with permission from Mochizuki, K. et al., Jpn. J. Appl. Phys. (In press). Copyright 2015 by the Japan Society of Applied Physics.)

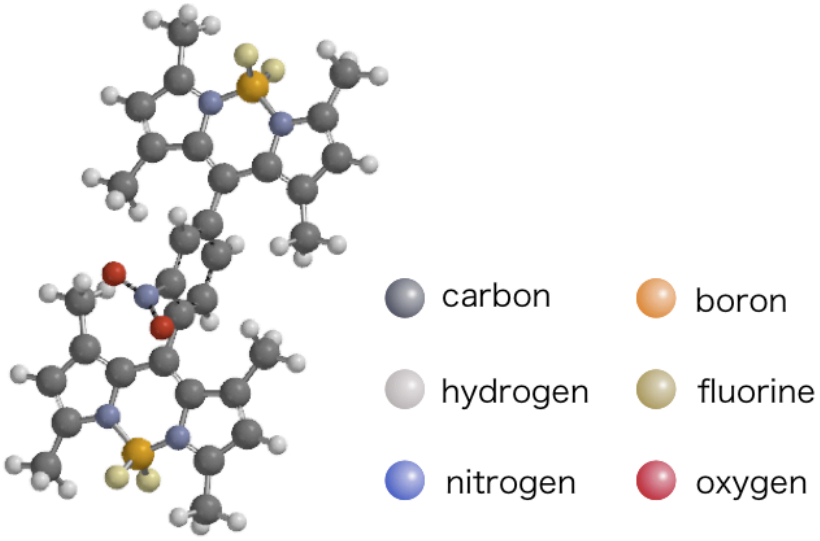

Fig. 3-3. The chemical structure of nitro-bisBODIPY drawn in ball & spoke model with **Spartan** (*Wavefunction*)

To accomplish the control experiment, two kinds of other compounds shown below were synthesized. One is a pair of one BODIPY and a nitro-benzene [nitro-monoBODIPY; D-A]. No fluorescence detection from this compound due to fluorescence quenching via PCS is expected. Synthesis of a similar compound was performed by T. Ueno et al. in 2006 and a quantum yield of 0.004 was reported [16]. The other is the pair of two BODIPYs and one benzene, resulting to the structure of two donors [bisBODIPY: D-D]. Because of the absence of the electron acceptor, this compound does not perform PCS. With this molecule, fluorescence response by two closely located BODIPYs can be investigated. The synthesis protocol is shown in the appendix chapter in this thesis. Optical properties including absorption spectra, emission spectra, molar absorption coefficients, fluorescence quantum yields of theses compounds are shown below.

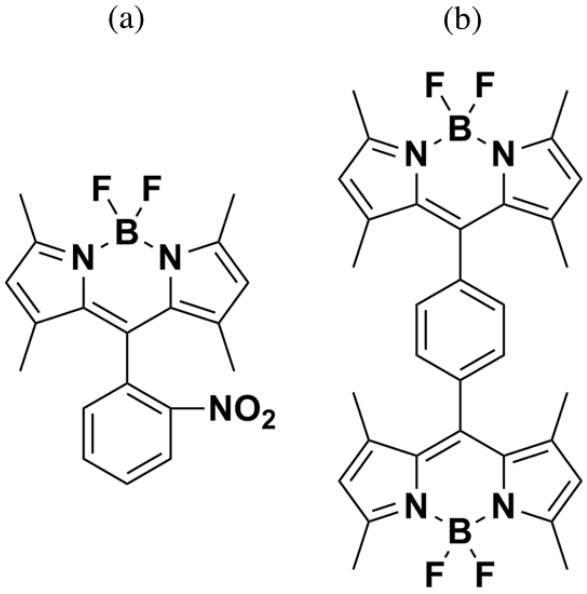

Fig. 3-4. The chemical structure of (a)nitro-monoBODIPY, (b)bisBODIPY. (Reprinted with permission from Mochizuki, K. et al., Jpn. J. Appl. Phys. (In press). Copyright 2015 by the Japan Society of Applied Physics.)

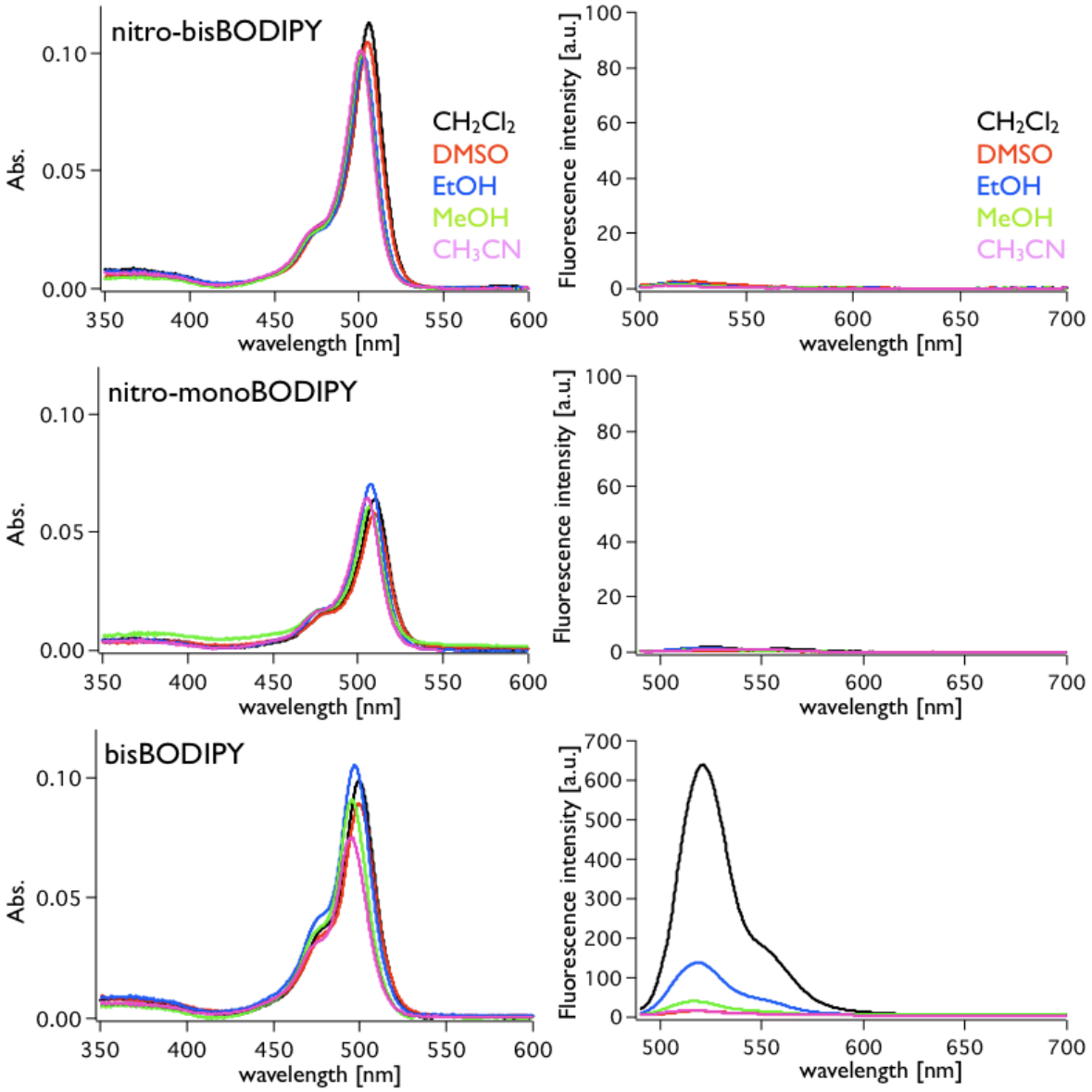

Fig. 3-5. Absorption and fluorescence spectra of nitro-bisBODIPY, nitro-monoBODIPY, bisBODIPY in various solvents with the concentration of 10 μM.

3.4 Measurement of the nonlinear fluorescence response

The nonlinear fluorescence response via PCS was experimentally confirmed. The fluorescence response against the increase of excitation intensity of the synthesized compounds was measured with a confocal microscope. According to the absorption spectra

of those compounds, they have absorption peak at around 500 nm. Therefore 488 nm CW light was chosen as excitation light source as trial (**Sapphire**, *Coherent*). 30 μm confocal pinhole which corresponds to around 0.5 airy unit size and water immersion oil (60x/1.2, *Olympus*) were used. The detection of fluorescence signal was conducted with avalanche photodiode (APD) (**SPCM-AQR-16**, *Optoelectronics*). The compounds were dissolved in methanol at a concentration of 10 μM after dissolved in cosolvents at 1 mM. As cosolvents, DMSO was used for BODIPY, nitro-bisBODIPY, nitro-monoBODIPY, and chloroform was used for bisBODIPY. The gate time of APD was 50 ms for each excitation intensities where the measurement was accumulated 5 times. The fluorescence responses of BODIPY and nitro-bisBODIPY are shown firstly below.

In double logarithmic graph, the slope exhibits the linearity of the relationship. Nonlinear relationship is described as slope of other than 1 whereas liner relationship is described with slope 1. In the nonlinear relationship, additionally, the value of slope means the order of nonlinearity. In the results, BODIPY showed clear linear response between fluorescence intensity and excitation intensity. On the other hand, nitro-bisBODIPY exhibited fluorescence response with the slope 2 in the range of high excitation intensity. In other words, nitro-bisBODIPY showed 2nd order nonlinear fluorescence response against the increase of excitation intensity. This supported that the absorption of two photons was involved in nitro-bisBODIPY to emit one fluorescence photon. What is noteworthy is that this fluorescence response was conducted with visible CW light excitation. In the low excitation intensity, nitro-bisBODIPY showed linear fluorescence response. This is presumably because the quantum yield of PCS is not 100 %, therefore a few compounds in the sample emit fluorescence with the one photon excitation process. Accordingly, the quantum yield of PCS decides the intensity of linear fluorescence response, which can be a background for the nonlinear response.

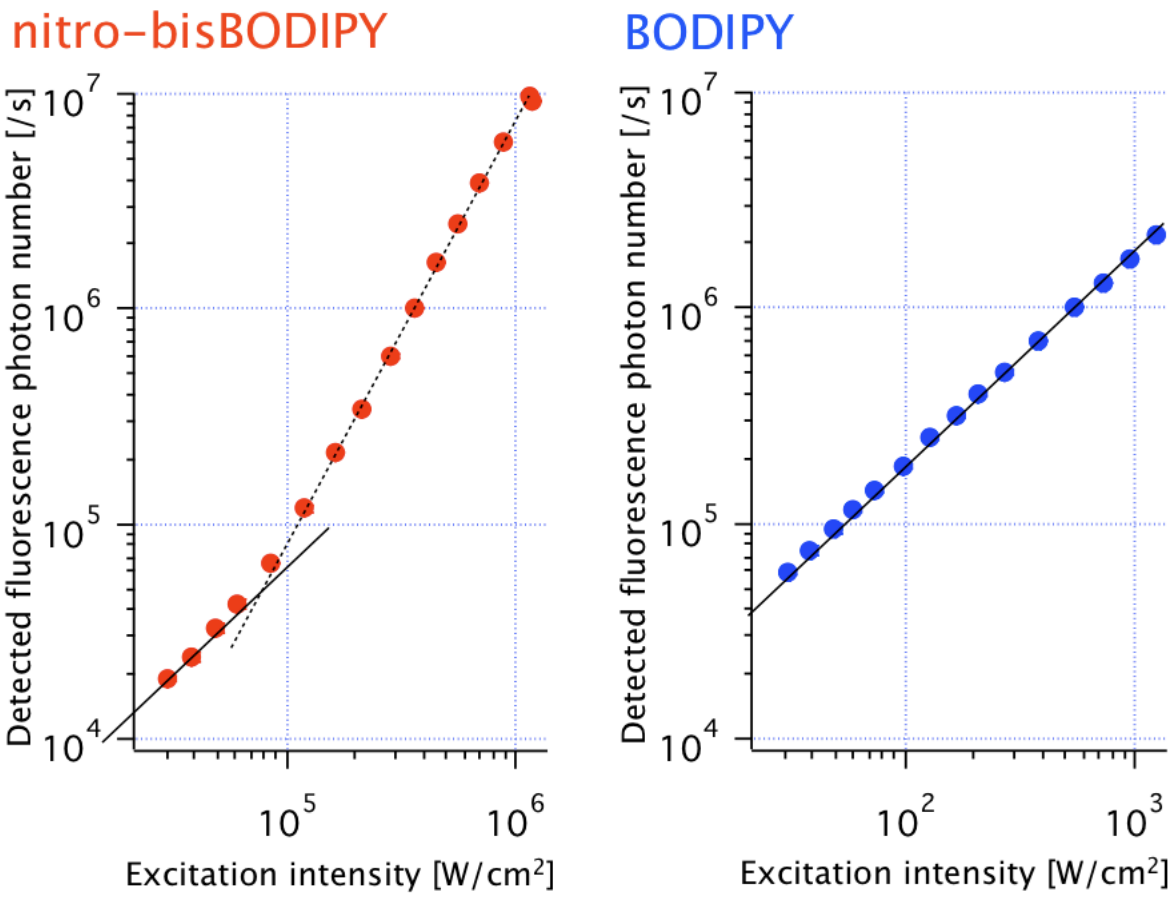

Fig. 3-6. Fluorescence response of nitro-bisBODIPY and BODIPY against the increase of excitation intensity shown in double logarithmic graph. The solid and dash lines represent functions with slope 1 and 2, respectively. Compounds were dissolved in methanol at the concentration of 10 μM and the measurements were conducted with laser scanning confocal microscopy with 488 nm CW excitation and a pinhole of 0.5 airy units. (Reprinted with permission from Mochizuki, K. et al., Jpn. J. Appl. Phys. (In press). Copyright 2015 by the Japan Society of Applied Physics.)

Next, the optical response of nitro-monoBODIPY and bisBODIPY is shown in Fig. 3-7. Nitro-monoBODIPY showed a weak liner fluorescence response. Comparing the fluorescence responses between BODIPY and nitro-monoBODIPY, the fluorescence intensity of nitro-monoBODIPY is lower than that of BODIPY with the difference of ~4000 times. This indicates that the suppression of fluorescence emission was performed

by the substitution of nitrobenzene, and its efficiency can be estimated as >99.9% from the difference of fluorescence intensity. And the intensity of a linear fluorescence response of nitro-monoBODIPY is consistent with that of nitro-bisBODIPY, which supports that the fluorescence quenching is efficiently performed also in the excitation process of nitro-bisBODIPY. On the other hand, bisBODIPY showed the linear fluorescence response with comparatively high fluorescence intensity. This has been also predicted because bisBODIPY consists of just two fluorophores and without electron transfers. However, fluorescence intensity of bisBODIPY is ~40 times lower than that of BODIPY. The decrease of fluorescence intensity can be explained by mainly two hypotheses. One is the decrease of molar absorbance coefficient (or absorption cross section). Second is the decrease in the quantum yield of fluorescence emission. From the aspect of molar absorbance coefficient, BODIPY and bisBODIPY showed almost same value that was around 1.0 x 10^5 $M^{-1}cm^{-1}$. Then the reason seems to be limited to the decrease of the quantum efficiency of fluorescence emission. The decrease of quantum yield of fluorescence emission is caused by the increase of rate constant of energy transitions other than fluorescence emission. If no occurrence of electron transfer is assumed in the relaxation process of bisBODIPY, the increase of rate constant of nonradiative decay (internal conversion) can be the main cause for the decrease of quantum yield of fluorescence emission as shown with next equation [4].

$$\Phi_{Fl} = k_{Fl} / (k_{Fl} + k_{IC}) \qquad (3\text{-}12)$$

, where k_{Fl}, k_{IC} denote the rate constant of fluorescence emission and internal conversion, respectively. This indicates that the close location of two fluorophores or the substitution of benzene for BODIPY cause the increase of rate constant of nonradiative decay. Therefore, the efficiency of PCS can be investigated by comparing fluorescence intensity of bisBODIPY and nitro-bisBODIPY. Judged from the experimental result, the difference in the fluorescence intensity of linear fluorescence response of bisBODIPY and nitro-bisBODIPY is approximately 100 times. Accordingly, the efficiency of fluorescence

suppression by PCS in nitro-bisBODIPY is estimated >99 %.

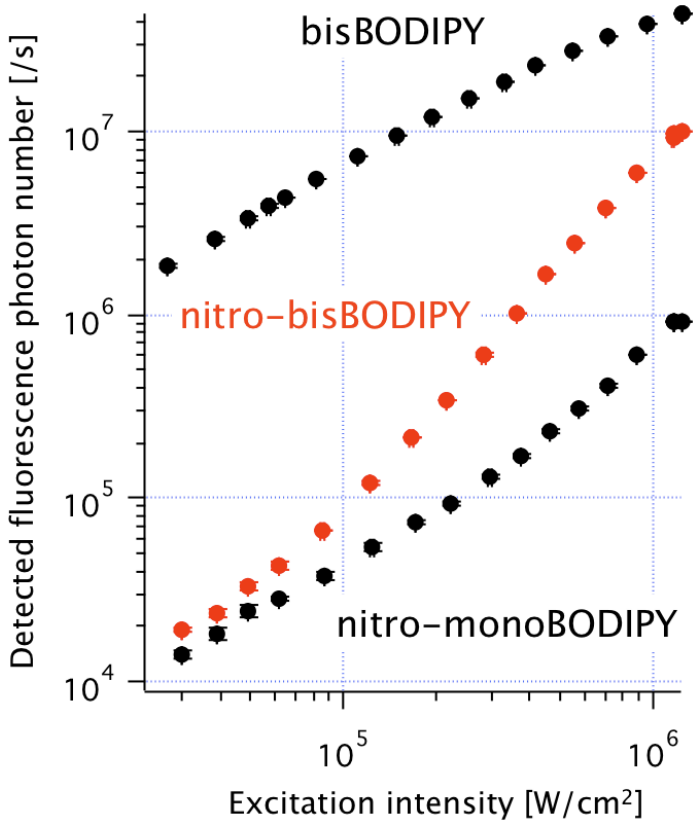

Fig. 3-7. Fluorescence response of nitro-bisBODIPY, nitro-monoBODIPY, bisBODIPY dissolved in methanol at the concentration of 10 μM. The measurements were conducted with laser scanning confocal microscopy with 488 nm CW excitation and a pinhole of 0.5 airy units. (Reprinted with permission from Mochizuki, K. et al., Jpn. J. Appl. Phys. (In press). Copyright 2015 by the Japan Society of Applied Physics.)

For more investigation, the solvent dependency of nonlinear fluorescence response and the dependence of the nonlinear response detection on the size of confocal pinhole were measured also. Figure 3-8(a) shows the fluorescence response of nitro-bisBODIPY in different solvent: methanol, ethanol, DMSO. The result showed that clear 2nd order nonlinear response of nitro-bisBODIPY was detected when they were dissolved in ethanol

as well as in methanol, but the blunting of the nonlinear fluorescence response was confirmed with compounds in DMSO. Fluorescence response of nitro-bisBODIPY in DMSO showed comparatively high linear response and the saturation with lower excitation intensity compared with the responses in methanol and ethanol. It seems that the property of solvents affects the quantum yield of PCS. Indeed, it has been known that the quantum yield o electron transfer strongly depends on polarity, viscosity of solvents [3]. Figure 3-8(b) shows the fluorescence response of nitro-bisBODIPY with different size of confocal detection pinhole. And in the result about the dependence on pinhole size, 2nd order nonlinear response was detected with any size of pinhole. Even without confocal pinhole, the nonlinear response was detected. The confocality worked to suppress the detection of linear florescence response and stray light from other than focus spot and consequently supported the detection of the nonlinear response.

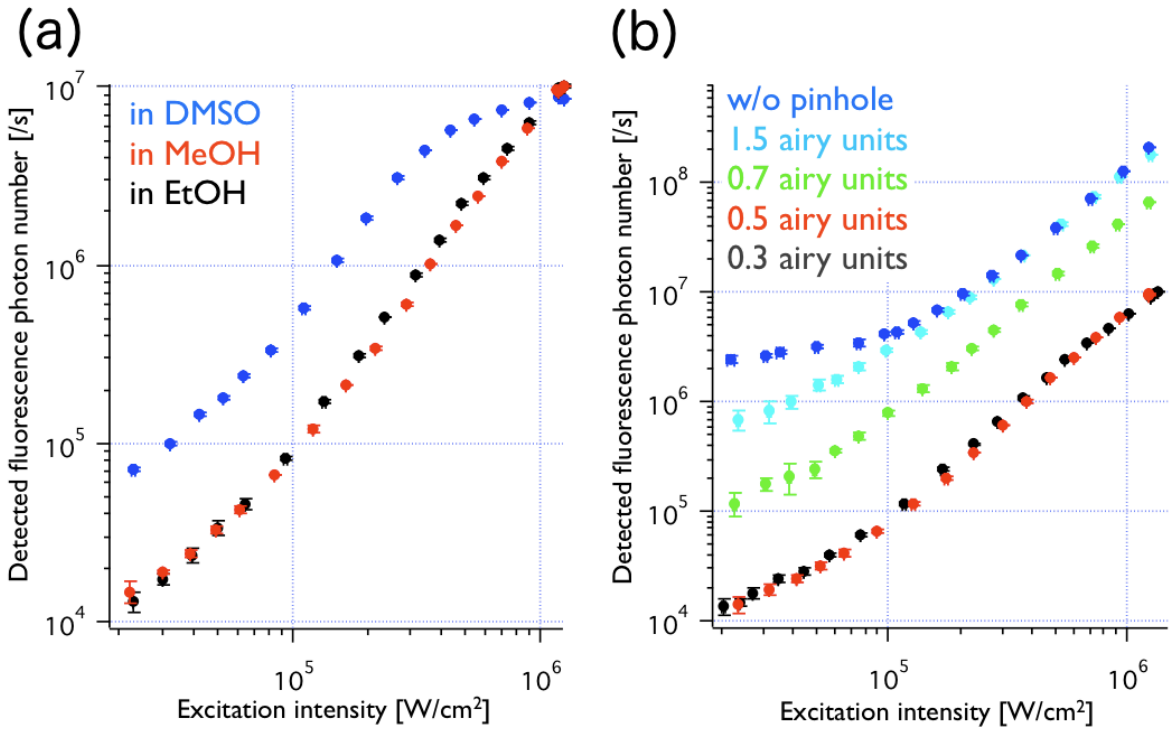

Fig. 3-8. (a)Fluorescence response of nitro-bisBODIPY dissolved in DMSO, ethanol, methanol at the concentration of 10 μM and a pinhole of 0.5 airy units. (b)Fluorescence response of nitro-bisBODIPY in MeOH (10 μM) measured with various sizes of confocal

pinhole. The measurements were conducted with laser scanning confocal microscopy with 488 nm CW excitation.

3.5 Super-resolution imaging of biological cells

The use of nitro-bisBODIPY in fluorescence imaging is expected to perform the improvement of spatial resolution since the 2nd order nonlinear fluorescence response was confirmed experimentally. It is noteworthy that the nonlinear fluorescence response was detected in confocal microscopy with 488 nm CW laser source, which indicated the strong possibility of super-resolution fluorescence imaging in the same confocal microscopy. In confocal microscopy, fluorescence imaging can be measured by laser scanning with maintaining the confocal effect. As explained in chapter 2, nonlinear fluorescence response makes the distortion of fluorescence PSF against the excitation PSF, which results in the improvement of the spatial resolution. Same as this mechanism, the use of nitro-bisBODIPY in laser scanning microscopy is expected to achieve spatial resolution improvement.

As a first step, I measured edge response of nitro-bisBODIPY solution. In the edge response measurement, the boundary of dye solution and glass substrates was imaged in the direction of excitation light propagation. 488 nm CW light source and water immersion objective lens (60x/1.2) was used, and the scanning was conducted by a galvanometer mirror scanning for x direction and a piezo stage scanning for z direction. The nitro-bisBODIPY and BODIPY was diluted in methanol at the concentration of 10 μM (DMSO was used as a cosolvent) at room temperature, and the dye solution was placed in glass bottom dishes. Below shows the vertical profiles in edge response images of the dye solution, averaged from the intensity in horizontal 256 pixles. Compared with the edge response with BODIPY, that of nitro-bisBODIPY showed a sharper change at the edge point, which indicates the improvement of spatial resolution. From the result, it was shown that the use of nitro-bisBODIPY enables us to obtain the spatial resolution improvement in fluorescence imaging.

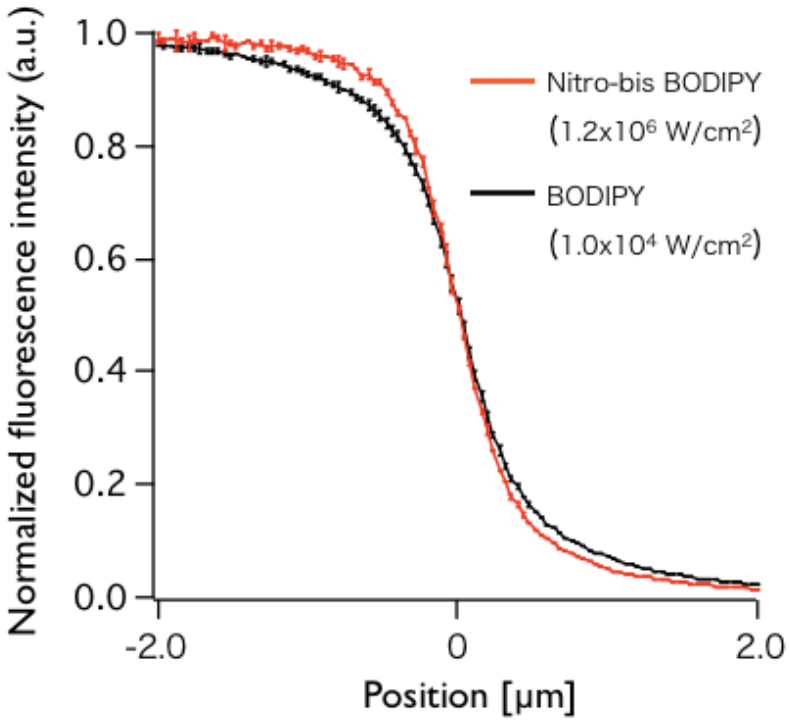

Fig. 3-9. Edge response of 10 μM nitro-bisBODIPY and BODIPY in methanol, where the fluorescence intensity of each position is averaged from the intensity of horizontal 256 pixels (Pixel size: 40 nm). The measurements were conducted with a laser-scanning confocal microscopy with 488 nm CW excitation.

Then I investigated the improvement of the spatial resolution in fluorescence images of biological cells by the use of nitro-bisBODIPY. BODIPY is well known as the lipophilic fluorescent dye and it can be used to stain oil storage in cells. The fluorescence images of lipid bodies in algal cells, lipid-containing vesicles in immortalized human hepatocytes, lipid droplets in mammalian cells by the use of BODIPY were reported [17-19]. In my experiment, HeLa cell which is a kind of human cancer cell was used as imaging target. Cells were immersed in 10 μM dye solution diluted with methanol at room temperature after two times washing by phosphate buffered saline (-). In this process, stain and fixation of cells are conducted simultaneously. After 30 minutes immersion, cells were washed out twice, and then filled up with methanol again. The fluorescence images of cells were

measured with a confocal microscope, water-immersion objective lens (60x/1.2), and excitation was conducted by a 488 nm CW laser. Figure 3-10 shows the XY and XZ fluorescence images of HeLa cells stained with nitro-bisBODIPY and BODIPY. Since different samples were compared, it was not easy to evaluate the resolution improvement quantitatively. However, comparison of the image contrast in the areas of the cell containing dense droplets shows the marked improvement in the quality of the image with nitro-bisBODIPY presumably as a result of the contrast enhancement or resolution improvement due to the nonlinear fluorescence response of the probe.

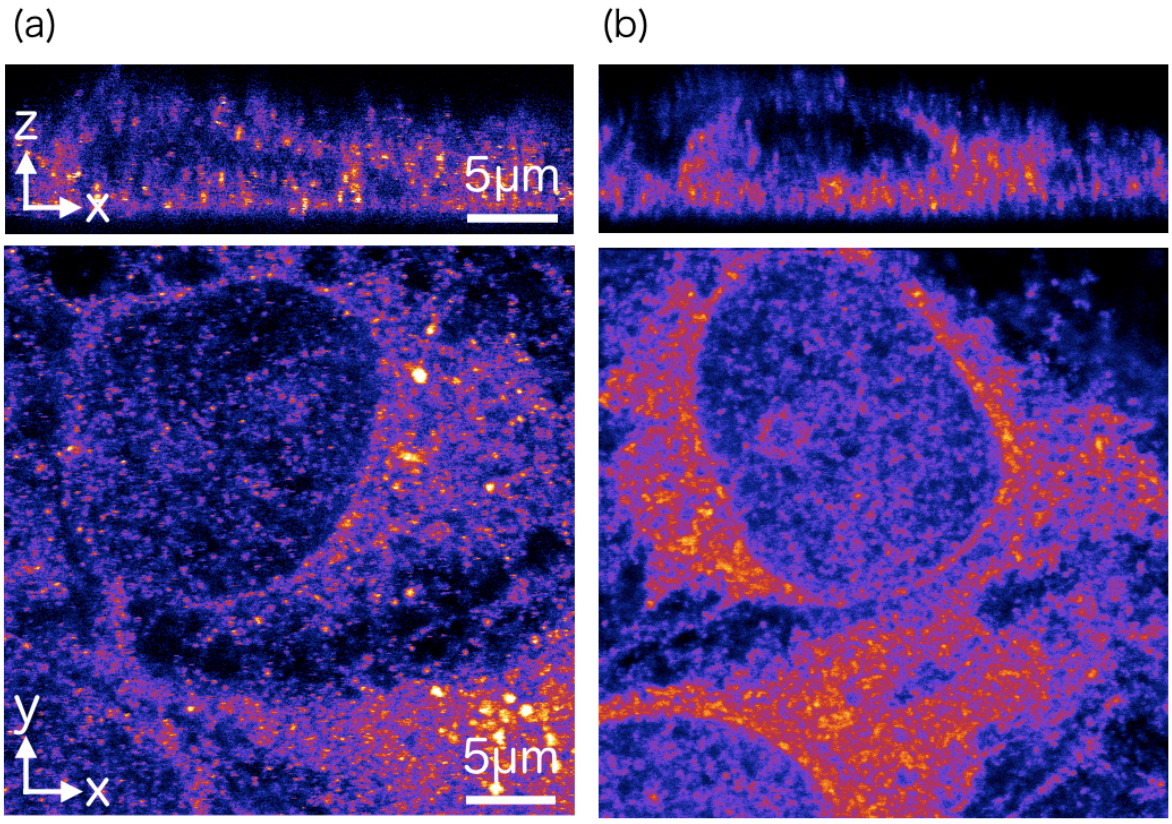

Fig. 3-10. Fluorescence images of HeLa cells stained with (a)nitro-bisBODIPY and (b)BODIPY (10 μM in MeOH) obtained with a laser scanning confocal microscope with 488 nm CW excitation. (Reprinted with permission from Mochizuki, K. et al., Jpn. J. Appl. Phys. (In press). Copyright 2015 by the Japan Society of Applied Physics.)

I also obtained fluorescence images of HeLa cells stained with bisBODIPY which chemical structure is more similar to nitro-bisBODIPY than BODIPY, and it was confirmed that the distribution of the probes and the image quality in terms of the contrast were similar to the image obtained with BODIPY. This supported the thing that nitro-bisBODIPY and BODIPY stains the same cellular organelles, therefore the improvement of image quality is given by the nonlinear fluorescence response of nitro-bisBODIPY but not the difference of intracellular materials which the probes stain.

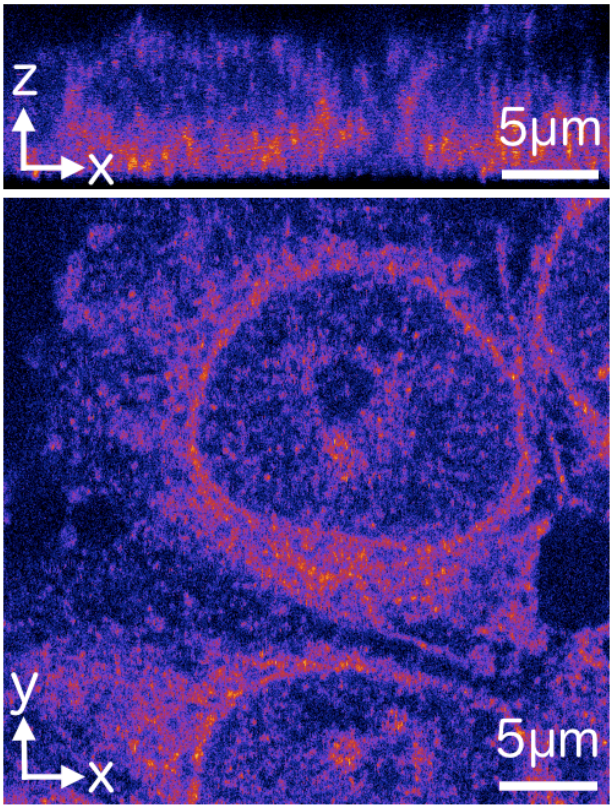

Fig. 3-11. Fluorescence images of HeLa cells stained with bisBODIPY (10μM in MeOH) measured with a laser scanning confocal microscope with 488 nm CW excitation.

Finally, nitro-bisBODIPY was applied to the improvement of spatial resolution in the fluorescence imaging using a conventional confocal microscope. For now I did not succeeded in evaluating the improvement of spatial resolution quantitatively, still the

practical utility of this probe in fluorescence imaging to realize higher spatial resolution was showed. What is noteworthy again is that this nonlinear fluorescence response can be achieved only using a laser-scanning (confocal) microscope with a visible-wavelength CW laser source. Due to the repetitive one-photon excitation, even visible-wavelength light achieved the nonlinear fluorescence response, and this allowed to maintain the resolution in laser-scanning confocal microscopy. Accordingly, the spatial resolution achieved using DUV-wavelength light is possible to be provided using a visible-wavelength light source and typical optical components. Accordingly, this nonlinear property of nitro-bisBODIPY or this concept of stepwise two-photon excitation is also be utilized for increasing the resolution of photolithography or density of optical data storage. And the excitation intensity required for 2nd order nonlinear fluorescence response is much lower than that of the typical TPEM which requires the use of pulsed light source. Moreover, it is predicted that temporal resolution in fluorescence imaging using nitro-bisBODIPY can be much improved by combined with the multi-focus system which is possible to be harnessed in a laser-scanning microscope.

References

[1] K. Mochizuki, L. Shi, S. Mizukami, M. Yamanaka, M. Tanabe, W.-T. Gong, A. F. Palonpon, S. Kawano, S. Kawata, K. Kikuchi, and K. Fujita, *Jpn. J. Appl. Phys.* (In press)

[1] 松林玄悦 著「化学結合の基礎 第二版」三共出版株式会社 (1999)

[2] G. J. Kavarnos, *"Fundamentals of Photoinduced Electron Transfer"* Wiley-VCH (1993)

[3] 御橋廣眞　編「蛍光分光とイメージングの手法」日本分光学会 (2006)

[4] J. R. Lakowicz, *"Principles of Fluorescence Spectroscopy Third Edition"* Springer (2006)

[5] P. E. Hänninen, L. Lehtelä, and S. W. Hell, *Opt. Comm.* **130**, 29 (1996).

[6] A. Schönle, P. E. Hänninen, and S. W. Hell, *Ann. Phys.* **8**, 115 (1999).

[7] J. Chen and Y. Cheng, *Opt. Lett.* **34**, 1831 (2009).

[8] F. Xu, L. Wei, Z. Chen, and W. Min, *Opt. Express* **21**, 14097 (2013).

[9] X. Zhu, Y. -T. Kao, and W. Min, *J. Phys. Chem. Lett.* **3**, 2082 (2012).

[10] M. S. Cooper, W. R. Hardin, T. W. Petersen, and R. A. Cattolico, *J. Biosci. Bioeng.* **109**, 198 (2010).

[11] H. Sunahara, Y. Urano, H. Kojima, and T. Nagano, *J. Am. Chem. Soc.* **129**, 5597 (2007).

[12] H. Lu, S. S. Zhang, H. Z. Liu, Y. W. Wang, Z. Shen, C. G. Liu, and X. Z. You, *J. Phys. Chem. A* **113**, 14081 (2009).

[13] Z. N. Sun, H. L. Wang, F. Q. Liu, Y. Chen, P. Kwong. H. Tam, and D. Yang, *Org. Lett.* **11**, 1887 (2009).

[14] T. Ueno, Y. Urano, K. Setsukinai, H. Takakusa, H. Kojima, K. Kikuchi, K. Ohkubo, S. Fukuzumi, and T. Nagano, *J. Am. Chem. Soc.* **126**, 14079 (2004).

[15] T. Ueno, Y. Urano, H. Kojima, and T. Nagano, *J. Am. Chem. Soc.* **128**, 10640 (2006).

[16] P. M. Cocze and D. A. Freeman, *Cytometry* **17**, 151-158 (1994)

[17] A. D. Gottardi, M. Vinciguerra, A. Sgroi, M. Moukil, F. R.-Dall'Antonia, V. Pazienza, P. Pugnale, M. Foti and A. Hadengue, *Lab. Invest.* **87**, 792-806 (2007)

[18] M. S. Cooper, W. R. Hardin, T. W. Petersen, and R. A. Cattolico, *J. Biosci. Bioeng.* **109**, 198-201 (2010).

Chapter4: Photophysical mechanism of nonlinear fluorescence response via PCS

Introduction

In this chapter, the theoretical analysis for nonlinear fluorescence response via PCS is performed. In the previous chapter, 2nd order nonlinear fluorescence response of nitro-bisBODIPY was confirmed experimentally and it was clear that the response occurred as results of the substitution of nitrobenzene for BODIPYs. For more investigation, I built a physical model of optical response of nitro-bisBODIPY and simulated the fluorescence response.

4.1 Physical model of the nonlinear fluorescence probe

The physical model about energy transition of nitro-bisBODIPY is proposed, which is composed of 5 energy states including charge-separated state as shown below. The predicted mechanism of the nonlinear fluorescence response via PCS was mentioned in chapter 3. One of BODIPY is excited by an incident photon and generates charge-separated state with nitro-benzene, and then only when the other BODIPY is excited by one more incident photon, finally nitro-bisBODIPY is allowed to emit fluorescence. Therefore the energy state of nitro-bisBODIPY is estimated to consist of a ground state [D-A-D], a excited state where one of BODIPY is excited [D*-A-D], a charge-separated state where the other BODIPY is in the ground state [D^+-A^--D] and another charge-separated state where another BODIPY is in the excited state [D^+-A^--D*]. Furthermore, nitro-bisBODIPY must has one more energy state where both BODIPYs in the compound are excited [D*-A-D*], which probability is so low that the value is calculated by the square of the probability of BODIPY excitation.

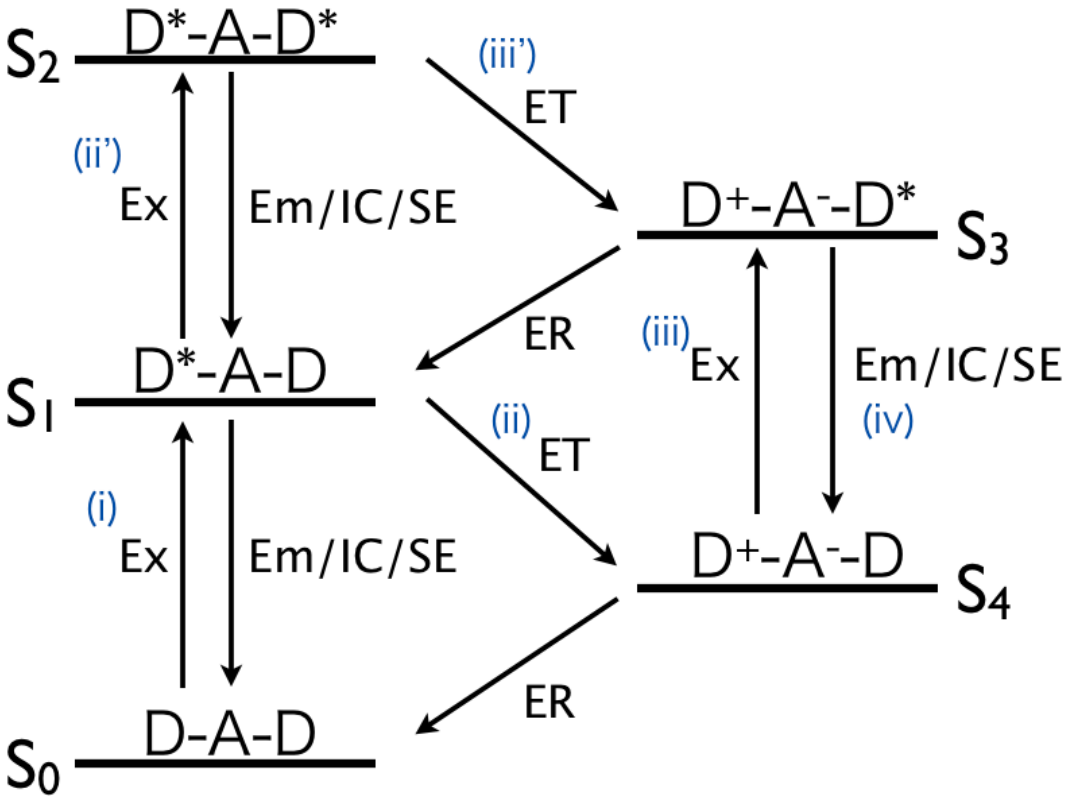

Fig. 4-1. Estimated energy states and molecular electronic transitions of nitro-bisBODIPY. Ex: excitation, Em: fluorescence emission, IC: internal conversion, SE: stimulated emission, ET: electron transfer, ER: electron recombination. (Reprinted with permission from Mochizuki, K. et al., Jpn. J. Appl. Phys. (In press). Copyright 2015 by the Japan Society of Applied Physics.)

In this model, energy transitions between each energy states are limited to excitation by incident photon [Ex], fluorescence emission [Em], internal conversion [IC], stimulated emission [SE], electron transfer [ET], electron recombination [ER] [1]. Intersystem crossing from the excitation states and photobleaching were ignored because these transitions make the energy diagram much more complicated. The nonlinear fluorescence response of nitro-bisBODIPY is expected to occur when the energy transition follows (i) ~ (iv) in Fig. 4-1 upon light excitation. (i)When one of the donors is excited by a photon in incident light, (ii)a charge-separated state is formed via intramolecular PCS. (iii)Then the

other donor can be excited by another incident photon while the charge-separated state is formed, and (iv)the probe emits a fluorescence photon finally. The simultaneous excitation of both donors (ii') and subsequent electron transfer to a charge-separated pair and an excited donor (iii') can be another possible pathway.

The accuracy of this model can be investigated by comparing the experimentally-detected fluorescence response and the simulated fluorescence response based on the model. Fluorescence response according to this physical model can be calculated by solving rate equations which describe the time-dependent population of the each energy state upon light excitation. In the simulation, some parameters are required including the absorption cross section of the compound and rate constants of each energy transition in the energy diagram. Absorption cross section was calculated from molar absorbance coefficient of nitro-bisBODIPY, which was experimentally given by the measurement of absorption spectra of the compound. However, the rate constants of fluorescence emission, internal conversion, and electron transfer/recombination were necessary to be estimated. Then I measured the transient absorption spectra of nitro-bisBODIPY.

4.2 Measurement of molecular electronic transition

In transient absorption spectra measurement, the energy transition of the specimen after light excitation can be traced by monitoring the change of absorbance [2]. From the change rate of absorbance, the rate constant of energy transitions can be estimated. Generally the pump-probe setup is used to measure the transient absorption spectra [3-7]. Absorbance change by light excitation can be achieved by the subtraction of absorption spectra before and after the excitation of the sample by ultrashort-pulsed light. The measurement of the absorbance change is measured temporally by delaying the measurement of absorption spectra after light excitation with the time span of picosecond ~ nanosecond range. The transient absorption spectra of nitro-bisBODIPY and bisBODIPY were measured from 0.1 ps after femtosecond pulsed light excitation to 8 ns.

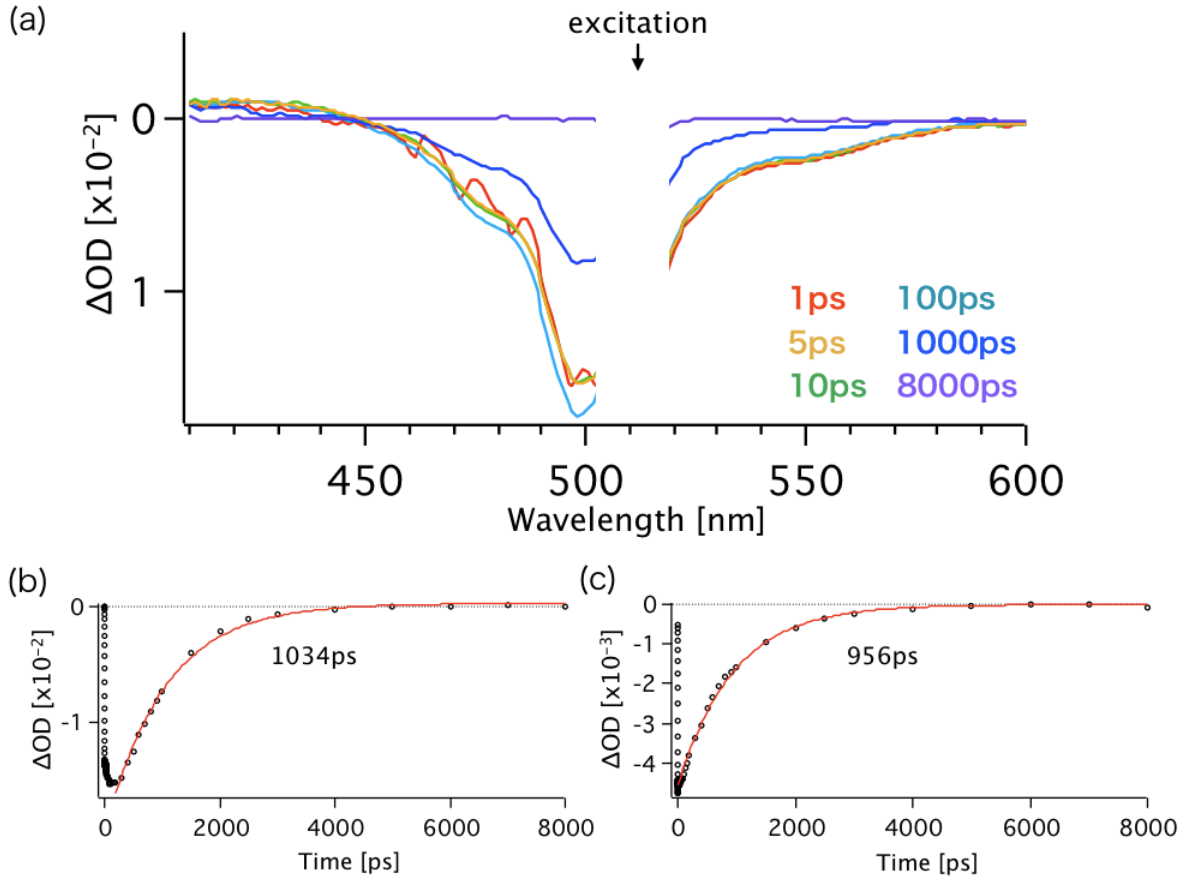

Fig. 4-2. (a)Transient absorption spectra of bisBODIPY after excitation with 510 nm femtosecond pulsed laser (1 ~ 8000 ps). Averaged time trace of absorbance changes of bisBODIPY in the wavelength of (b)490~500 nm and (c)520~540 nm are also shown. (Reprinted with permission from Mochizuki, K et al., Jpn. J. Appl. Phys. (In press). Copyright 2015 by the Japan Society of Applied Physics.)

In the result of bisBODIPY, only a negative absorbance change was detected at around 490 ~ 500 nm which corresponds to the wavelength range of absorption peak. From this absorbance change, the population of ground state can be monitored. The decay of ground state can be detected as the decrease of absorbance in the range, and the return of the ground state can be detected as the recovery of it. In the case of bisBODIPY which consists only of fluorophores, it can be assumed that the decay and recovery of the ground state is equivalent to the excitation transition to the excited state and the relaxation transition to the

ground state, respectively. The time trace of the absorbance change of bisBODIPY averaged at around the absorption peak (490 ~ 500 nm) is shown in Fig. 4-2(b) . Here, the time traces of these absorbance changes were analyzed by fitting mono- or bi-exponential decay functions shown below [8].

$$F(t) = A + a_1\exp\{-(t - t_1) / \tau_1\} + a_2\exp\{-(t - t_2) / \tau_2\}+.... \quad (4\text{-}1)$$

, where A, a_n, t_n, τ_n denote the constant, value of the actual maximum absorbance change, temporal offset value, the time constant. And we can choose the degree of fitting function by changing the number of n. The time constant of targeted absorbance change can be described with τ_n acquired in the fitting process, which represents the time where the absorbance change becomes $1/e$ of its maximum. Therefore, the time constant of the targeted molecular energy transition contributing to the absorbance change is also acquired with τ_n. As the result of fitting process, $(1\ \text{ns})^{-1}$ was calculated as the rate constant in the relaxation transition for bisBODIPY while around $(1\ \text{ps})^{-1}$ was calculated as the rate constant in the excitation transition for the compounds. The rate constant of relaxation transition is also described as the lifetime of the excited state. And about the time constant of the excitation process, the value of 1 ps is estimated to almost the resolution limit in the measurement. The time constant of molecular excitation transition is known to be in the order of femtosecond [9]. The acquisition of the value of 1 ps in the measurement is thought to be the result of convolution with the pulsed light excitation which has certain temporal bandwidth (Around 500 fs is estimated as the final bandwidth of excitation single pulse in this measurement.) Therefore, the time constant of the excitation transition can be described as <1 ps. And the rate constant is defined as the reciprocal of the time constant shown as below [10].

$$k = 1 / \tau \quad (4\text{-}2)$$

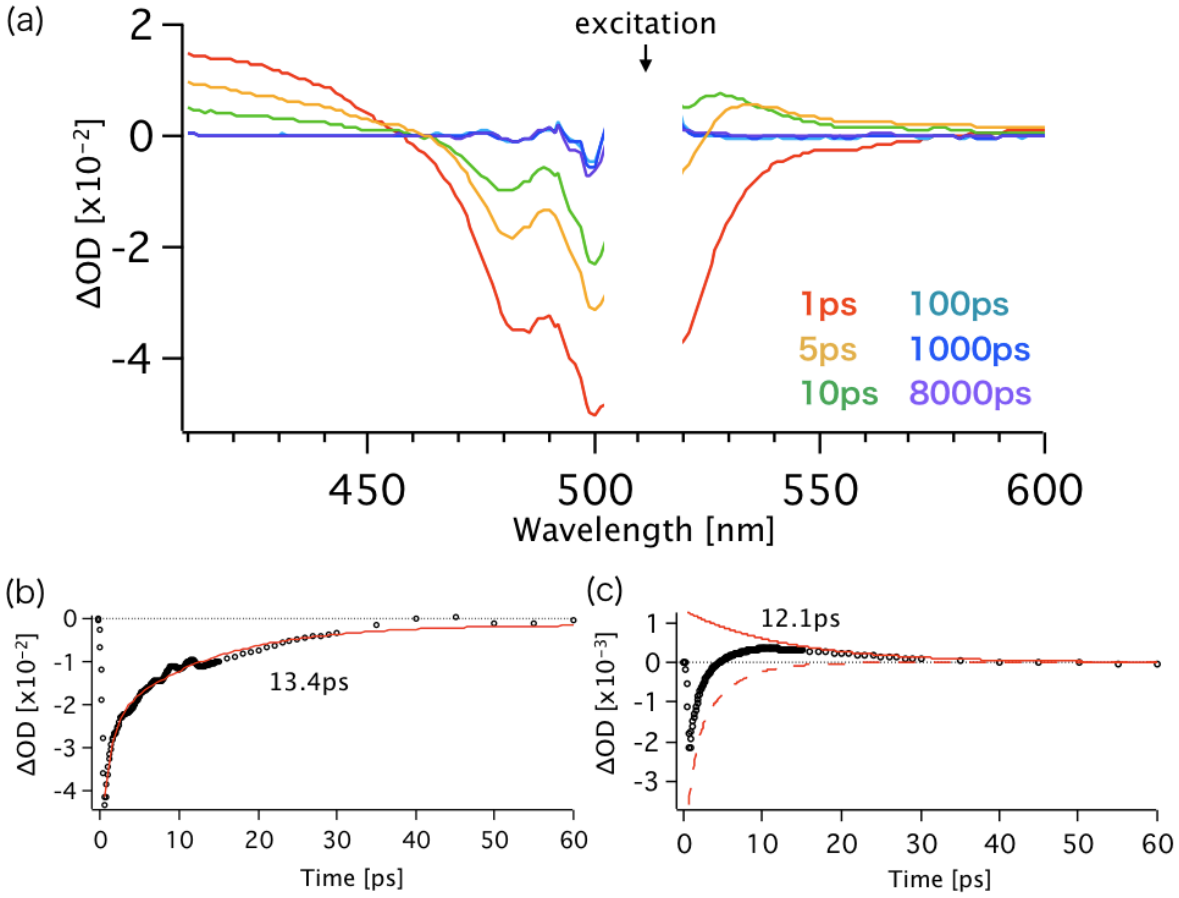

Fig. 4-3. (a)Transient absorption spectra of nitro-bisBODIPY after excitation by 510 nm femtosecond pulsed laser (1 ~ 8000 ps). Averaged time trace of absorbance changes of nitro-bisBODIPY in the wavelength of (b)490~500 nm and (c)520~540 are also shown. (Reprinted with permission from Mochizuki, K. et al., Jpn. J. Appl. Phys. (In press). Copyright 2015 by the Japan Society of Applied Physics.)

In summary, it was obtained that bisBODIPY in the ground state was excited with the rate constant of $>(1\ \mathrm{ps})^{-1}$ after light excitation, then go back to the ground state with the rate constant of around $(1\ \mathrm{ns})^{-1}$. Compared with the rate constant for relaxation process of BODIPY ($\sim(5\ \mathrm{ns})^{-1}$), that of bisBODIPY provided higher value. Because the measured rate constant for the relaxation process from the excited state is equal to the summation of rate constants of natural fluorescence relaxation and internal conversion as shown below, it is estimated that the increase of the relaxation rate constant of bisBODIPY is derived from the

increase of the rate constant for internal conversion [10].

$$k_{\text{Relaxation (measured)}} = k_{\text{Fl}} + k_{\text{IC}} \qquad (4\text{-}3)$$

The increase of the rate constant for internal conversion is presumably caused due to the close location of two fluorophores as discussed in the last chapter. Then the energy diagram of bisBODIPY can be described with two energy states including the ground state and excited state.

Finally the transient absorption spectra of nitro-bisBODIPY are investigated. Two negative and two positive absorbance changes were observed at around 480 nm, 500 nm and 420 nm, 530 nm, respectively. Since the wavelength of 480 and 500 nm correspond to the local maximum points in absorption spectrum of nitro-bisBODIPY, the bleaching and recovery of the ground state after excitation can be monitored from the absorbance change at these wavelengths. Figure 4-3(b) shows the averaged time trace of absorbance changes in the wavelength of 490 ~ 500 nm. Immediately after the excitation by a single pulse light, the molecule starts losing the absorbance and approaching the maximum within 1 ps. This absorbance loss recovers with the lifetime of 13 ps, which indicates the presence of a short-lived excitation state in nitro-bisBODIPY in contrast to the long-lived one of BODIPY and bisBODIPY. This strongly suggested that PCS occurred instead of the fluorescence emission soon after nitro-bisBODIPY was light-excited. Next, the positive transient band around 530 nm was investigated. This positive absorbance change is assumed as the result of generation and decay of the charge-separated state only the BODIPY dyes with a nitrobenzene showed this transient band, but not confirmed in the spectra of BODIPY and bisBODIPY. In fact, Hattori et al. reported that the relatively weak positive peak in this range is attributed to the generation of radical cation of BODIPY moiety [11]. The average time trace of absorbance change in the wavelength of 520 ~ 540 nm was monitored as shown in Fig. 4-3(c). Since the contribution of absorbance loss due to ground state bleaching still remains at this time scale, the time trace was fitted with bi-exponential decay functions with positive and negative coefficients. The absorbance

change in the wavelength of 520 ~ 540 nm quickly rises soon after excitation and reaches the maximum within 1 ps, and then decaying with the lifetime of 12 ps. This result implies that the charge-separated state is generated within 1 ps after light excitation and has a lifetime of 12 ps. Combined with the result from monitoring the ground state, the energy transitions of nitro-bisBODIPY after a single pulse excitation can be summarized as follows. After excitation, the energy state of nitro-bisBODIPY transits to the excited state (<1 ps). Then it changes to the charge-separated state within 1 ps via PCS. Finally, the molecule changes back to the ground state after 12 ps lifetime of the charge-separated state. It can be assumed that the nonlinear fluorescence response occurs only when one more photon is absorbed by the molecule through the other donor within this 12 ps lifetime of the charge-separated state. The positive absorbance change around 420 nm presumably shows the generation and decay of the excited state because other dyes including BODIPY and bisBODIPY showed the same response. However, it was difficult to detect the transition rate because the wavelength region overlaps with the absorption peak of the radical anion of nitrobenzene [12].

Now the rate constants for the generation and decay of the charge-separated state can be acquired as the reciprocal of the time constant of them, resulting to $>(1\ \text{ps})^{-1}$ and $(12\ \text{ps})^{-1}$, respectively. And these exactly correspond to the rate constants for electron transfer (k_{ET}) and electron recombination (k_{ER}) which are the one of parameters needed for the simulation of fluorescence response. The rate constants for fluorescence emission and internal conversion of nitro-bisBODIPY were impossible to be detected from its transient absorption spectra. Therefore, I decided to refer the rate constant for the relaxation process of bisBODIPY, which is the summation of the rate constant for fluorescence emission and internal conversion as discussed above.

4.3 Simulation of the nonlinear response

After the measurement of parameters needed for the simulation of fluorescence response was given, the calculation of rate equation based on the model is conducted. The rate equation based on the model is shown below.

$$\frac{dS_0}{dt} = -k_{Ex}S_0 + (k_{Em} + k_{IC} + k_{SE})S_1 + k_{ER}S_3$$

$$\frac{dS_1}{dt} = k_{Ex}S_0 - (k_{Ex} + k_{Em} + k_{IC} + k_{SE} + k_{ET})S_1 + (k_{Em} + k_{IC} + k_{SE})S_2 + k_{ER}S_4$$

$$\frac{dS_2}{dt} = k_{Ex}S_1 - (k_{Em} + k_{IC} + k_{SE} + k_{ET})S_2$$

$$\frac{dS_3}{dt} = k_{ET}S_1 - (k_{Ex} + k_{ER})S_3 + (k_{Em} + k_{IC} + k_{SE})S_4$$

$$\frac{dS_4}{dt} = k_{Ex}S_3 + k_{ET}S_2 - (k_{Em} + k_{IC} + k_{SE} + k_{ER})S_4$$

Total fluorescence intensity of nitro-bisBODIPY by light excitation can be explained as the rate of population in the excited state which is stochastically consumed by fluorescence emission. The rate is described as “the rate constant for fluorescence emission” of “the summation of the rate constant for all energy transition” in each excited state. And the model contains three excited state, therefore the fluorescence intensity is calculated by the summation of population for fluorescence emission of those excited state. The calculation was conducted with a calculation software (**Matlab,** *Mathworks*). As mentioned in the previous section, the value of >$(1ps)^{-1}$ and $(12ps)^{-1}$ were assigned to the rate constant of electron transfer and electron recombination. Figure 4-4 shows the simulation results of fluorescence response based on the estimated model about nitro-bisBODIPY with various rate constant values of electron transfer: $(0.5ps)^{-1}$, $(0.4ps)^{-1}$, $(0.3ps)^{-1}$, $(0.2ps)^{-1}$, $(0.1ps)^{-1}$, $(0.01)^{-1}$ whereas the rate constant of electron recombination was fixed to $(12ps)^{-1}$. When k_{ET} is small, the quantum yield of PCS is low and this results in the increase of linear fluorescence component. To compare the simulation results with the experimental results, I focused to the blue square region in Fig. 4-4(a), which is equivalent to the excitation intensities used in the experiment. In this region, the simulated fluorescence response in which k_{ET} is $(0.2\ ps)^{-1}$ exhibits a second-order nonlinear response that is well consistent with the experimental result. Consequently $(0.2\ ps)^{-1}$ can be a good estimation for the rate constant of electron transfer of nitro-bisBODIPY. The time duration of 12 ps is enough for

nitro-bisBODIPY to be interacted with a second incident photon after absorbing the first incident photon even in the condition of excitation by visible CW source while a typical two-photon absorption molecule requires an pulse light source to realize simultaneous two-photon absorption within femtosecond order [13,14].

I calculated the fluorescence response of nitro-bisBODIPY also by changing the value of k_{ER} to provide more investigation to nonlinear fluorescence response via PCS (Fig. 4-4(b)). The calculation result showed that the second-order nonlinear response is generated with lower excitation intensity with smaller k_{ER}. When k_{ER} is large, the charge-separated state seems to dissolve before absorption of the second incident photon. As shown in the plot with k_{ER} = (1.2 ps)$^{-1}$, the 2nd-order nonlinear response is generated at higher excitation intensity where absorption of the second photon can occur before the molecule recovers to the ground state.

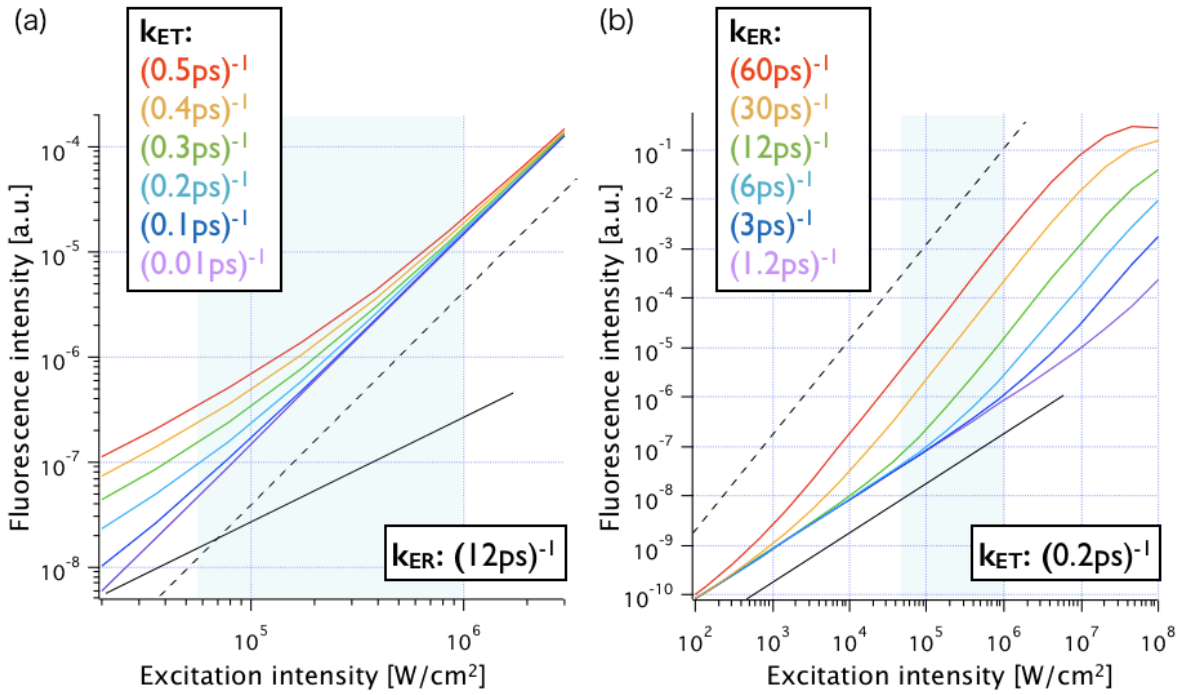

Fig. 4-4. Fluorescence response of nitro-bisBODIPY simulated by referring the estimated energy diagram of nitro-bisBODIPY with different rate constants of (a)electron transfer (k_{ET}) and (b)electron recombination (k_{ER}). The dashed and solid lines are shown with slope 2 and

1, respectively. (Reprinted with permission from Mochizuki, K. et al., Jpn. J. Appl. Phys. (In press). Copyright 2015 by the Japan Society of Applied Physics.)

From the investigations described above, the chemical modification of nitro-bisBODIPY or the selection of a different pair of electron donor-acceptor may contribute to increase the lifetime of the charge-separated state nonlinear, thereby realizing fluorescence response with much lower excitation intensity. Simultaneously, the use of different combinations of fluorophores or electron acceptors instead of BODIPY and nitrobenzene can be attempted to enhance fluorescence signal intensity. Furthermore, it is also predicted for this strategy that the order of nonlinearity in fluorescence response can be increased by increasing the number of charge-separated pair formed in a prbe.

References

[1] C. Eggeling, A. Volkmer, and A. M. Seidel, *ChemPhysChem* **6**, 791-804 (2005)

[2] G. J. Kavarnos, "*Fundamentals of Photoinduced Electron Transfer*" Wiley-VCH (1993)

[3] A. Harriman, J. P. Rostron, M. Cesario, G. Ulrich, and R. Ziessel, *J. Phys. Chem. A* **110**, 7994-8002 (2006)

[4] A. N. Amin, *J. Phys. Chem. A* **115**, 9810-9819 (2011)

[5] K. Flavin, K. Lawrence, J. Bartelmess, M. Tasior, C. Navio, C. Bittencourt, D. F. O'Shea, D. M. Guldi, and S. Giordani, *ACS NANO* **5**, 1198-1206 (2011)

[6] J.-Y. Liu, M. E. El-Khouly, S. Fukuzumi, and D. K. P. Ng, *Chem. Asian J.* **6**, 174-179 (2011)

[7] A. Eggenspiller, A. Takai, M. E. El-Khouly, K. Ohkubo, C. P. Dros, C. Bernhard, C.Goze, F. Denat, J. -M. Barbe, and S. Fukuzumi, *J. Phys. Chem. A* **116**, 3889 (2012).

[8] G. Jones II, S. Kumar, O. Klueva, and D. Pacheco, *J. Phys. Chem*. *A* **107**, 8429 (2003).

[9] 御橋廣眞　編「蛍光分光とイメージングの手法」日本分光学会 (2006)

[10] J. R. Lakowicz, "*Principles of Fluorescence Spectroscopy Third Edition*" Springer (2006)

[11] S. Hattori, K. Ohkubo, Y. Urano, H. Sunahara, T. Nagano, Y. Wada, N. V. Tkachenko, H. Lemmetyinen, and S. Fukuzumi, *J. Phys. Chem. B* **109**, 15368 (2005).

[12] G. Duvanel, N. Banerji, and E. Vauthey, *J. Phys. Chem. A* **111**, 5361 (2007).

[13] A. Diaspro, "*Confocal and Two-Photon Microscopy*" Wiley-Liss (2002)

[14] W. Denk, J. H. Strickler, and W. W. Webb, *Science* **248**, 73-76 (1990)

Chapter 5: Nonlinear fluorescence response via spirocycle opening

Introduction

In this chapter, 3rd order nonlinear fluorescence response by visible light excitation is shown. In chapter 3 and 4, the 2nd order nonlinear fluorescence response via PCS was investigated and applied to super-resolution fluorescence imaging. Here, I present stepwise three-photon excitation by visible light excitation using spirocyclic compounds. The accomplishment of this technique is expected to achieve more resolution improvement than 2nd order nonlinear response via PCS.

5.1 Spirocyclic compounds

A part of spiro compounds such as spiropyran have photochromism which is switched with the spirocycle opening and closing [1,2]. Photochromism is defined as a reversible transformation of a compound induced by light absorption between two forms with different absorption spectra [3,4]. And the spirocyclic compound is a collective term indicating organic compounds with two rings connected with one atom. Recently, the photochromism of rhodamine spiroamide (RSA) is being marked due to some reports in the field of super-resolution microscopy.

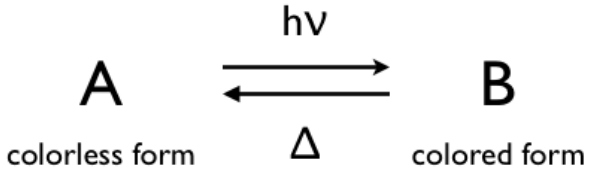

Fig. 5-1. Schematic showing photochromism of a molecule via light excitation (h ν) and thermal relaxation or light excitation with different wavelength (Δ).

The research group of S. W. Hell reported the upgrade of a localization microscopy by

the use of modified RSA [5,6]. The photochromism of RSA had been already reported by K.-H. Knauer et al. in 1977 [7], however more investigations for it have not been given for a long time because of its low quantum yield, the low thermal stability of the open isomer, the low reputation limit of spirocycle opening/closing. They succeeded in improving these shortcomings of RSA by developing a new RSA based on Rhodamine B which is known as a fluorophore with quite high thermal stability [5]. In their research, 4-Aminophthalimide was conjugated to rhodamine B, thus forming a spirocycle with high absorbance for UV wavelength excitation. And high thermal stability of the open isomer was realized by the substitution of a carbonyl group, which has strong electron withdrawing property. Then they used this RSA as a fluorescent probe in a localization microscopy and realized the upgrade of the spatial resolution and temporal resolution because of the improved thermal stability of the open isomer, which induce the huge contrast of fluorescence intensity between the open and closed isomers. Additionally, they performed the optical sectioning in a thick sample (>6μm) by activating the probes to ON state with two-photon excitation, where the excitation wavelength was 747 nm against the absorption wavelength of closed isomer was <350 nm.

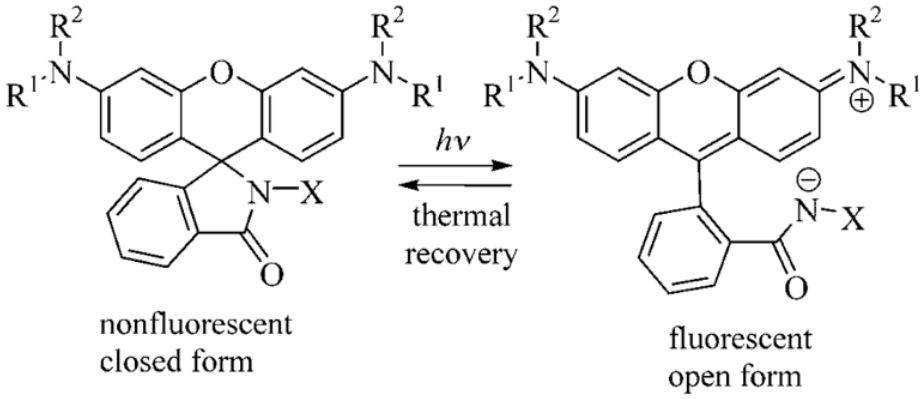

Fig. 5-2. Schematic showing photochromism of RSA. Reprinted with permission from WILEY-VCH Veriag GmbH & Co.: V. N. Belov et al., *Chem. Eur. J.* **15**, 10762-10776 (2009).

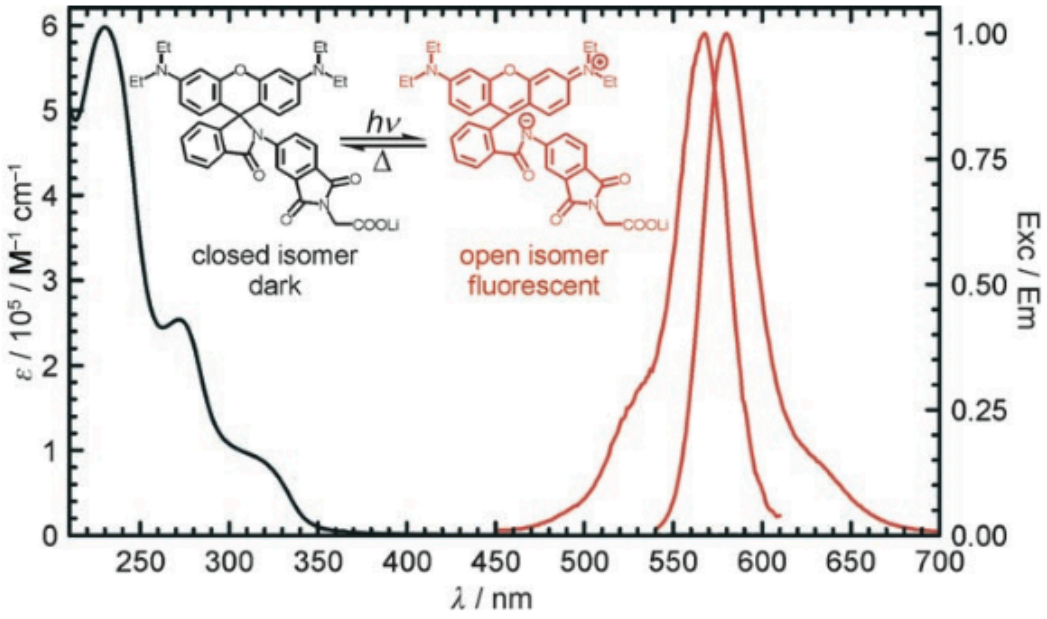

Fig. 5-3. Absorption spectra of closed isomer of RSA and absorption/emission spectra of open isomer of RSA [6]. Reprinted with permission from WILEY-VCH Veriag GmbH & Co.: J. Fölling et al., *Angew. Chem. Int. Ed.* **46**, 6266-6270 (2007).

Other than RSA, some other type of spirocyclic compounds providing photochromism were developed recently. HySOx was invented as a result of the research to control the fluorescence of tetramethylrhodamine (TMR) [8]. TMR is known as useful fluorescent probe with significant photochemical and photothermal properties even in aqueous solution, high emission intensity, high molecular extinction coefficient ($1x10^5$ $M^{-1}cm^{-1}$), independence from pH changes and tolerance for photobleaching [9]. HySOx is one of thiol analogs of HMTMR (hydroxymethyltetramethylrhodamine), which was synthesized by substituting the carboxyl groups in TMR, aiming to optimize the thermal stability of the spirocyclic compounds. As results, HySOx is perfectly colorless and non-fluorescent in aqueous solution with a wide range of pH values. And the release from the spirocyclic form occurs by the oxidation of the S atom. HySOx was tested as the fluorescence probe to detect HOCL for biological conditions.

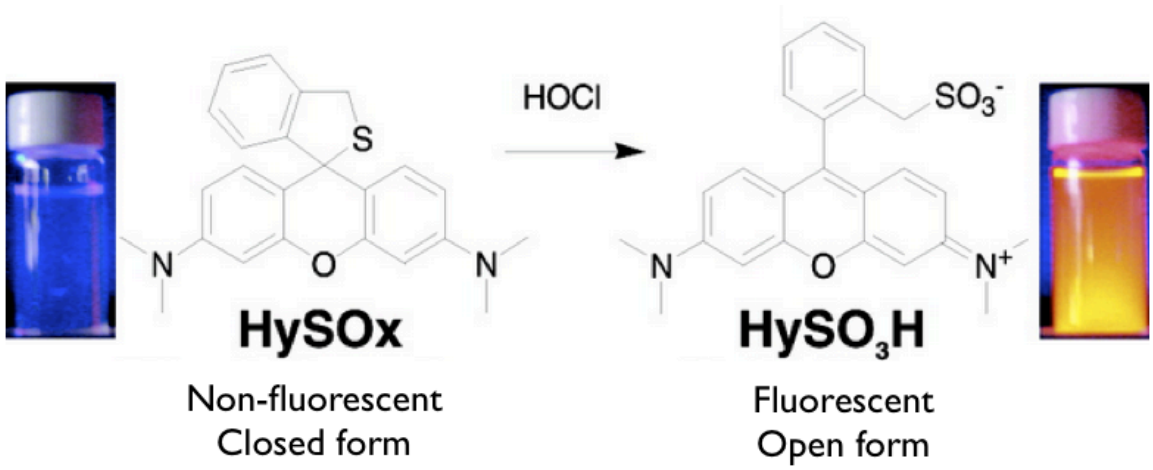

Fig. 5-4. The schematic showing spirocycle opening of HySOx. Reprinted with permission from American Chemical Society: S. Kenmoku et al., *J. Am. Chem. Soc.* **129**, 7313-7318 (2007)

And MMSiR was established as HOCl detection probe operating in the near-infrared region which realizes low phototoxicity, low background due to less autofluorescence, and high tissue penetration in biological applications [10-11]. The mechanism to detect HOCl used in HySOx was applied to Si-rhodamine which has absorption and fluorescence peaks at around 650 nm.

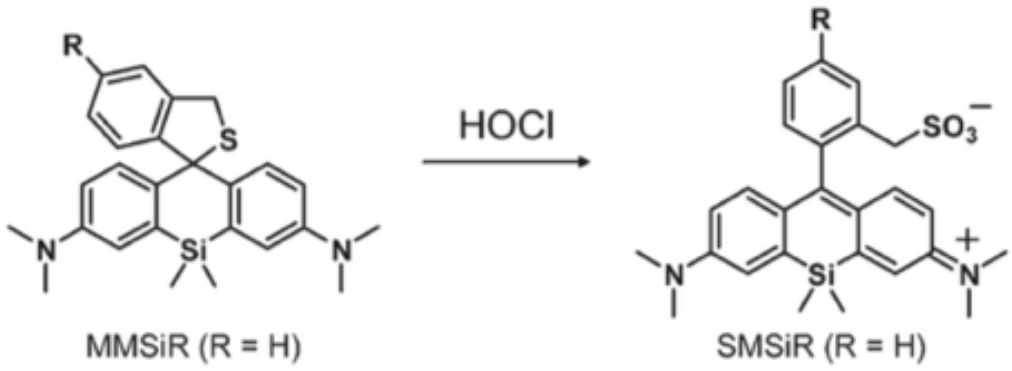

Fig. 5-5. Structural formula of MMSiR. Reprinted with permission from American Chemical Society.: Y. Koide et al., *J. Am. Chem. Soc.* **133**, 5680-5682 (2011)

The spirocyclic compounds such as HySOx, MMSiR used for the HOCl detection are

known to react ring opening/close also via light irradiation [12]. Considering these compounds, I propose another strategy to realize nonlinear fluorescence response with visible-wavelength excitation.

5.2 Stepwise three-photon excitation

It is predicted that stepwise three-photon excitation is realized by the use of spirocyclic compounds. The achievement of 3rd order fluorescence response with a visible wavelength excitation enables us to realize the super-resolution fluorescence microscopy with a laser scanning microscopy. The concept of stepwise three-photon excitation with spirocyclic compounds is described with two consecutive processes, which are two-photon excitation for spirocycle opening to switch them to fluorescent state and subsequent one-photon excitation for fluorescence emission as shown below.

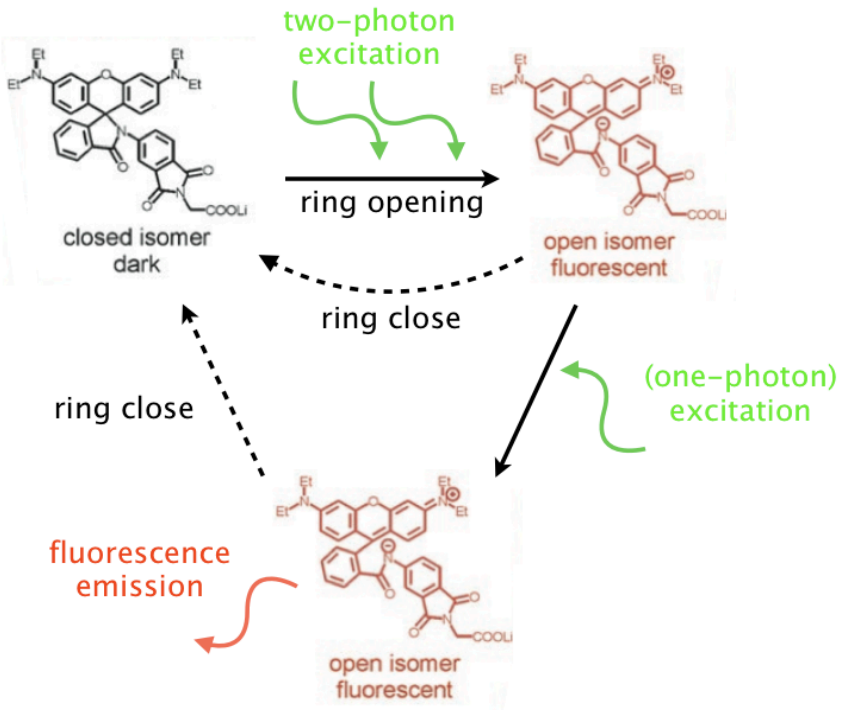

Fig. 5-6. Schematic explaining the concept of stepwise three-photon excitation of a spirocyclic compound (RSA) by the visible-wavelength pulsed light excitation. The chemical

structure of RSA in the figure is referred from. Adapted with permission from WILEY-VCH Veriag GmbH & Co.: J. Fölling et al., *Angew. Chem. Int. Ed.* **46**, 6266-6270 (2007)

The accordance of the wavelength for two-photon excitation and one-photon excitation is required for this concept. As introduced in the previous section, some of spirocycle compounds have absorption in UV wavelength to be switched to ON state (fluorescent state, open form) from OFF state (non-fluorescent, closed form) and in visible wavelength to be fluorescence-excited (see Fig. 5-6). By the excitation with visible wavelength, therefore, there is a strong possibility to achieve both two-photon excitation in UV range and one-photon excitation in visible range. The use of pulsed light source is estimated to be necessary for this stepwise three-photon excitation, accurately for the achievement of two-photon absorption in the UV wavelength range. And what is noteworthy is that those excitations are required to occur in a same quantum event. Accordingly, one-photon absorption for fluorescence excitation after two-photon excitation is needed to realize while the compound is in ON (fluorescent) state.

The occurrence of the stepwise three-photon absorption can be evaluated from the detection of 3rd order nonlinear fluorescence response. Then the experiments were done to measure fluorescence response of spirocyclic compounds excited with visible-wavelength pulsed light source. FLIP 565 (one of RSA), HySOx, MMSiR, which were introduced in the previous section, were chosen as candidates of the nonlinear fluorescence probe [12].

5.3 Measurement of 3rd order nonlinear fluorescence response

The fluorescence responses of FLIP 565, HySOx, MMSiR excited by visible-wavelength pulsed light source were measured. The setup is based on a laser scanning confocal microscopy with pulsed excitation. The detection of fluorescence intensity was performed with APD in this research also. The 780 nm pulsed laser (80 MHz, 200 fs) provided by Titanium-Sapphire laser (**MaiTai**, *Spectra-Physics*) was tuned to desired visible wavelengths with an optical parametric oscillator (**Inspire**, *Spectra-Physics*). Since FLIP 565 and HySOx have the absorption peaks for fluorescence excitation in the

wavelength around 550 nm and MMSiR has it around 650 nm [6, 12], the excitation wavelength of 510, 530, 550 nm for FLIP 565, HySOx and 610, 630, 650 nm for MMSiR were used. Although two-photon excitation was involved in this experiment, the isolation of excitation light and fluorescence was accomplished with long-pass edge filter because the fluorescence excitation is conducted with one-photon excitation process. And the 3 types of solvents (pH 7.4 buffer, pH 11 buffer, methanol) were used to measure fluorescence response of the spirocyclic compounds. This is because that the fraction of the number of the open isomer and closed isomer in equilibrium condition is reported to depend on the surrounding condition such as pH of solvents. Under the use of HySOx, it was shown that higher absorbance and fluorescence intensity of the compound in equilibrium condition were detected in lower pH buffer solution because of the increase of the number of open isomer [8]. Lower fraction of the number of the open isomer is expected in the measurement because the linear fluorescence response by the open isomer should be suppressed to detect 3rd order nonlinear fluorescence response. The concentration of the compounds was 10 μM in each solvent. The gate time of APD was 250 ms for each excitation intensity where the detection was accumulated 5 times. The objective lens of 60x/1.2 (water immersion) was used and pinhole size corresponded to the 0.5 airy disk size.

As results, 3rd order nonlinear fluorescence responses were detected with MMSiR. To clarify the detection of 3rd order nonlinear response by MMSiR, the fluorescence response of MMSiR in pH11 buffer solution excited with 610 nm pulsed is shown (see Fig. 5-7). The 3rd order nonlinear response appeared after the linear response showed saturation against the increase of excitation intensity. In other words, the photon density higher than that for saturation of MMSiR is needed for realization of the 3rd order nonlinear response.

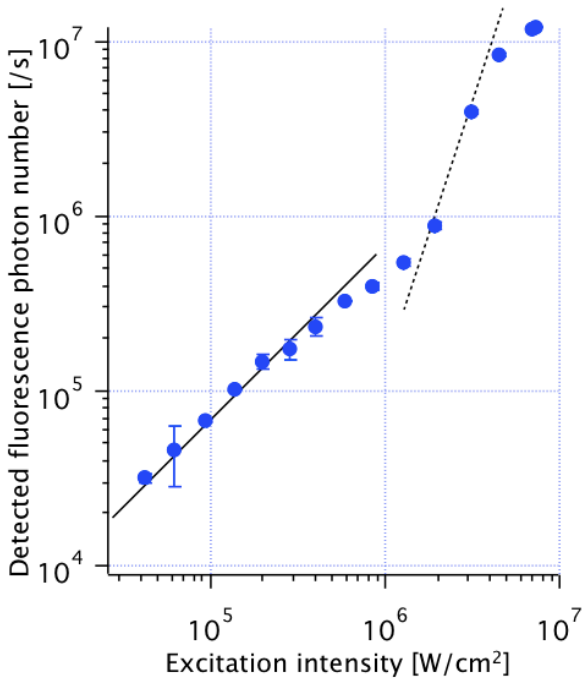

Fig 5-7. Fluorescence response of MMSiR (10 μM in pH11 buffer solution) excited with 610 nm pulsed laser. The solid and dash lines indicate slope 1 and 3, respectively.

Then the fluorescence responses of all RSA, HySOx, MMSiR is shown below. In the measurement of fluorescence response of RSA and HySOx with 510 ~ 550 nm pulsed excitation, only linear responses were detected, in which no recovery of fluorescence intensity after their saturation was detected. On the other hand, MMSiR provided nonlinear fluorescence response by excited with 610, 630 nm pulsed light source. Especially the 3rd order response was confirmed with MMSiR which were dissolved in buffer solution and excited with 610 nm pulsed. And that was given with wide range of excitation intensity when they were dissolved in the buffer of pH 11. This can be explained by the decrease of linearly emitted fluorescence due to the decrease of the number of the open isomer in equilibrium condition in the higher pH solvent. This is supported by that the higher fluorescence photon number of fluorescence response from MMSiR in pH 7.4 buffer solution. As the reason of the detection of less than 3rd order response from MMSiR in

methanol, it is presumably thought that the number of open isomers in equilibrium condition was increased or the lifetime of open isomer was so decreased that they returned to closed form before the accomplishment of one-photon absorption for fluorescence emission. Up to 2nd order nonlinear response was given with MMSiR solved in methanol. This result supports the possibilities that the number of the open isomer in the equilibrium condition increased or the lifetime of them decreased in the condition in organic solvents. And the non-detection of nonlinear fluorescence response with FLIP 565 and HySOx is considered with two reasons. One is the high number of the open isomer, as described above. And another is that the spirocycle opening didn't occur well by the excitation with under 550 nm pulsed excitation. Considered from the second reason, it must be worth to measure fluorescence responses of HySOx or RSA with pulsed light of other wavelengths than 510 ~ 550 nm such as 610 nm in order to realize the 3rd order nonlinear fluorescence response.

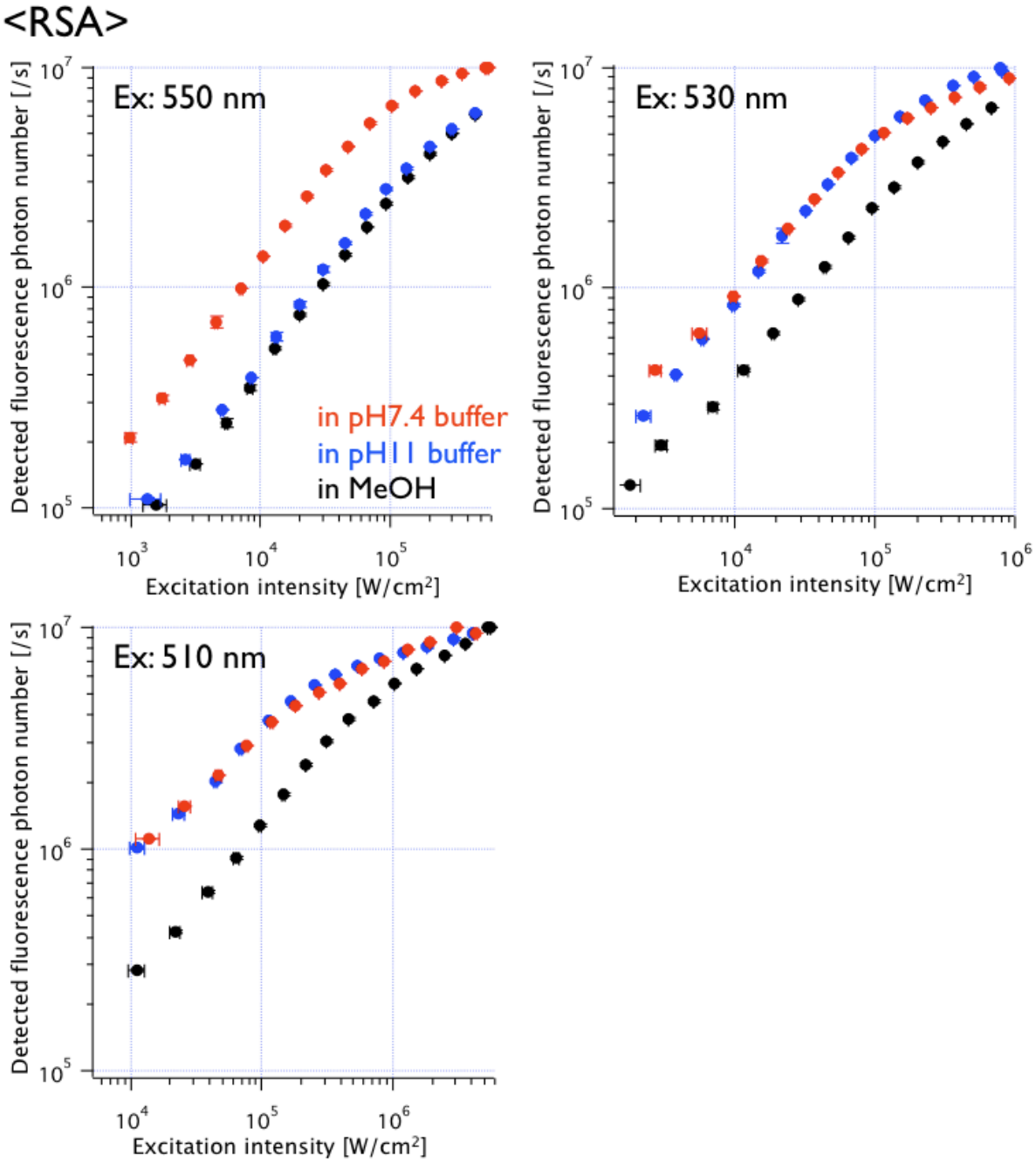

Fig. 5-8. Fluorescence response of RSA (10 μM in MeOH and pH 7.4, 11 buffer solution) excited with 510 ~ 550 nm pulsed laser. Only linear fluorescence response was detected and it showed saturation at the high excitation intensity.

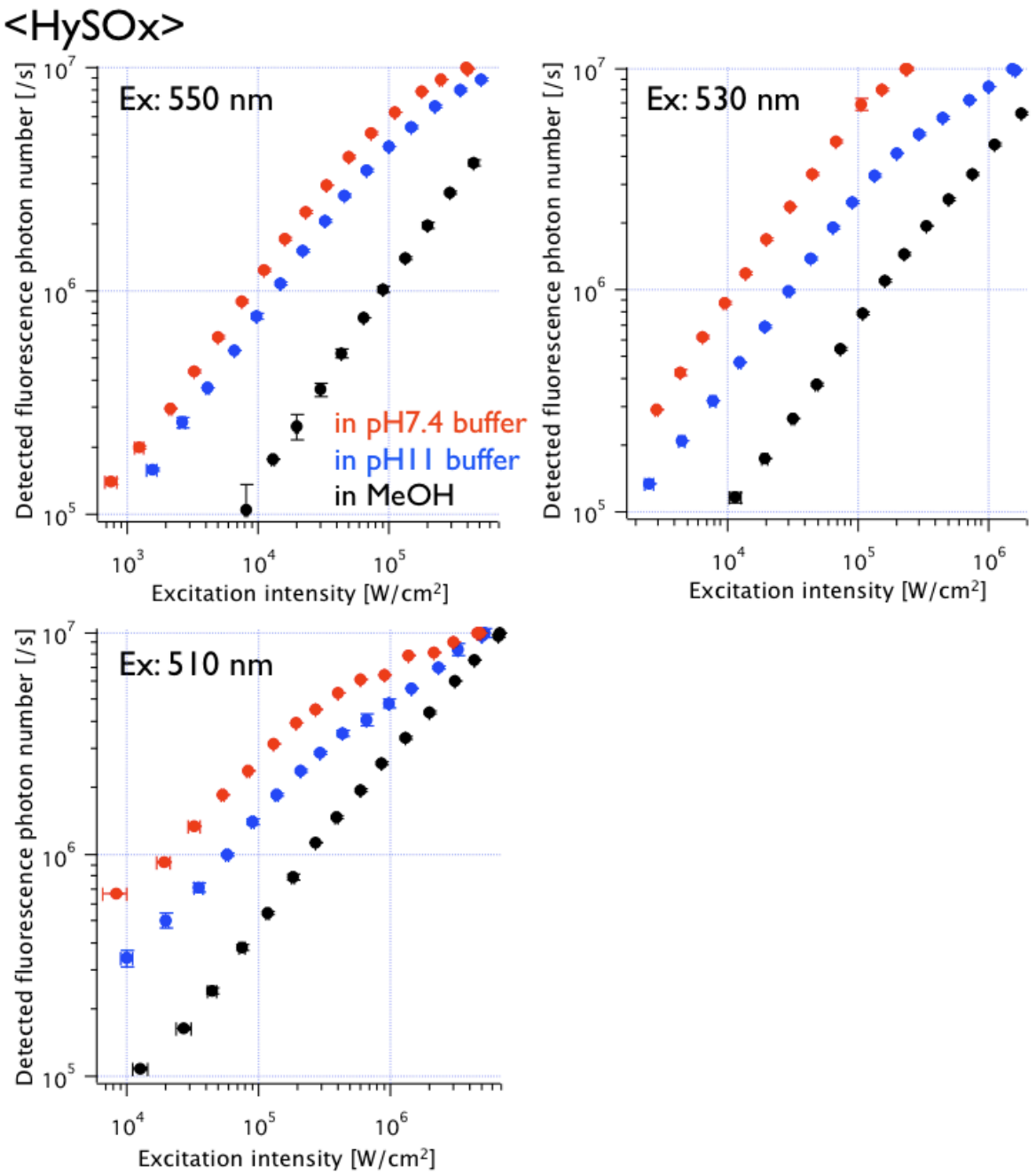

Fig. 5-9. Fluorescence response of RSA (10 μM in MeOH and pH 7.4, 11 buffer solution) excited with 510 ~ 550 nm pulsed laser. Only linear fluorescence response was detected and it showed saturation at the high excitation intensity.

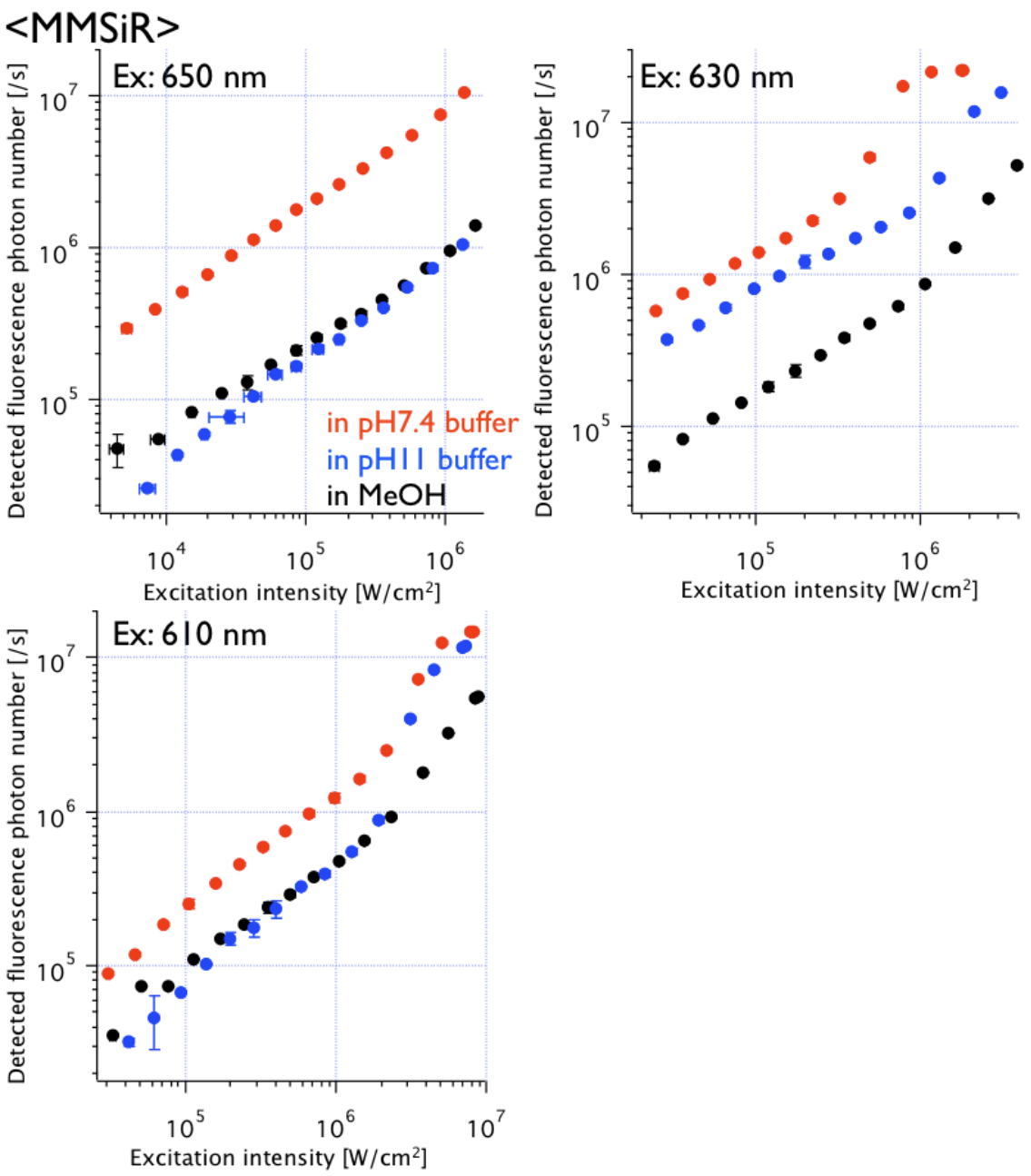

Fig. 5-10. Fluorescence response of MMSiR (10 μM in MeOH and pH 7.4, 11 buffer solution) excited with 610 ~ 650 nm pulsed laser. Nonlinear fluorescence responses were provided after the saturation of linear response.

Also about MMSiR, the range of excitation intensities providing the 3rd order nonlinear response is considered too short to achieve the resolution improvement in fluorescence imaging by laser-scanning. Therefore it is required to optimize the experimental condition in measurements of the 3rd order nonlinear fluorescence of MMSiR, including the excitation wavelength as the outlook of this research. For now, however, the strong possibility to realize the super-resolution fluorescence imaging by using spirocyclic compounds were indicated, in which a 1.7 fold improvement of spatial resolution is expected compared with the conventional confocal microscopy.

References

[1]日本化学会　編「有機フォトクロミズムの化学」学会出版センター (1996)

[2] E. Fischer, *Chemie in unserer Zeit* **9**, 85-95 (1975)

[3] G. H. Brown, "*Photochromism*" Wiley-Intersciences (1971)

[4] M. Heilemann, P. Dedecker, J. Hofkens, and M. Sauer, *Laser & Photon. Rev.* **3**, 180-202 (2009)

[5] V. N. Belov, M. L. Bossi, J. Fölling, V. P. Boyarskiy, and S. W. Hell, *Chem. Eur. J.* **15**, 10762-10776 (2009)

[6] J. Fölling, V. Below, R. Kunetsky, R. Medda, A. Schönle, A. Egner, C. Eggeling, M. Bossi, and S. W. Hell, *Angew. Chem. Int. Ed.* **46**, 6266-6270 (2007)

[7] K. H. Knauer and R. Gleiter, *Angew. Chem. Int. Ed. Engl.* **16**, 113 (1977)

[8] S. Kenmoku, Y. Urano, H. Kojima, and T. Nagano, *J. Am. Chem. Soc.* **129**, 7313-7318 (2007)

[9] N. P-Voloshina, R. P. Hauglnad, J. B-Stewart, M. K. Bhalgat, P. J. Millard, F. Mao, W.-Y. Leung, and R. P. Haugland, *J. Histochem. Cytochem* **47**, 1179-1188 (1999)

[10] Y. Koide, Y. Urano, K. Hanaoka, T. Terai, and T. Nagano, *J. Am. Chem. Soc.* **133**, 5680-5682 (2011)

[11] Y.-Q. Sun, J. Liu, X. Lv, Y. Liu, Y. Zhao, and W. Guo, *Angew. Chem. Int. Ed.* **51**, 7634-7636 (2012)

[12] S. Uno, M. Kamiya, T. Yoshihara, K. Sugawara, K. Okabe, M. C. Tarhan, H. Fujita, T. Funatsu, Y. Okada, S. Tobita, and Y. Urano, *Nature Chem.* **6**, 681-689 (2014)

Chapter 6. Probe development for super-resolution Raman microscopy of intracellular materials

Introduction

In the previous chapters, the development of probes for super-resolution fluorescence microscopy was shown. The new concept to modify the fluorescence probes provided advantages in fluorescence microscopy which have not been achieved by the modification of optical setup. In this chapter, I applied this concept based on "the modification of probes" to super-resolution Raman microscopy. Raman microscopy is also widely used in biology and medicine same as fluorescence microscopy. For the realization of this purpose, I investigated a technique to fabricate SERS probes inside cells, using laser-induced photoreduction [1]. The probe was composed of gold nanostructures and worked as the probes to enhance Raman scattering of cellular materials by the plasmon resonance.

6.1 Surface enhanced Raman scattering (SERS)

Raman scattering is possible to be enhanced by the use of localized surface plasmon resonance (LSPR) induced by metallic nanostructures. Detection of Raman scattering from atoms, molecules, which is known as Raman spectroscopy, informs us not only the spatial distribution of them but also molecular structural or environmental information. One of shortcomings in Raman spectroscopy is weakness of signals derived from the quite low absorption cross section of Raman scattering. Raman scattering was discovered as a new type of light scattering from light-irradiated molecules in 1928 [2]. Raman scattering is generated as the result of molecular or electronic oscillation of molecules although it is generated with a Rayleigh scattering which is generated by dipolar oscillation of molecules [3]. While wavelength of Rayleigh scattering is same as that of excitation light, Raman scattering contains slightly-shifted wavelengths due to the energy loss via molecular or electronic oscillation of molecules. Therefore, spectral information of Raman scattering along the wavelength shifted from that of excitation light depends of the structure of

targeted atoms or molecules because each atom or molecule has different combination of molecular or electronic oscillation. Accordingly, it is possible to identify the unknown targets or to detect the structural/environmental changes of them by the detection of their Raman scattering. However, one of shortcomings of Raman scattering or Raman spectroscopy is the weak signals or low quantum yield of them. This has ever been solved by the use of localized surface plasmon resonance of metallic nanostructures.

The enhancement of Raman scattering is realized by the excitation of target materials with the enhanced electromagnetic field, which is generated in the vicinity of metallic nanostructures by LSPR [4]. When metal nanostructures are excited by electromagnetic radiation under resonant conditions, they exhibit collective oscillations of their conduction electrons named localized surface plasmon [5]. This electron oscillation by selective photon absorption is called LSPR, and is known to cause enhancement of local electromagnetic field or scattering. The wavelength which corresponds to the maximum resonance for the LSPR is highly dependent on the size, shape and configuration of the nanostructures [6,7].

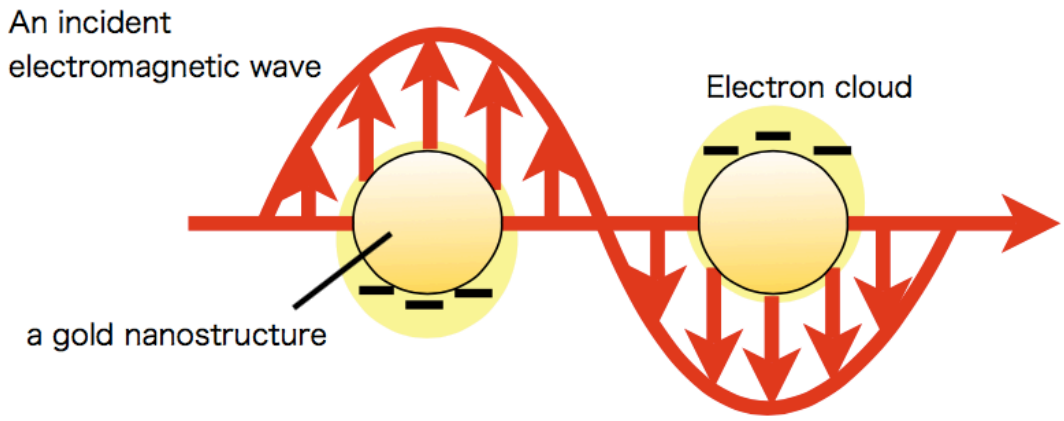

Fig. 6-1. The schematic of collective oscillation of free electron around metal nano-particles exited by incident light.

By excited with this strong electromagnetic field, materials near around NPs show more intensive optical response such as fluorescence, Raman scattering than them

generated through the normal excitation way. Because of its nano-sized configuration, moreover, targets to be excited are limited in a few nanometers, resulting to the dramatic decrease of noise signals and the improvement of optical resolution. Surface Enhanced Raman Scattering (SERS), which was firstly found by Fleischman in 1974, is a phenomenon which Raman scattering of molecules adsorbed on rough metal surface or metallic nanostructures is enhanced [8-10]. In 1978, Martin Moskovits proposed that the large increase in Raman cross section was derived from the surface plasmon resonance [11]. This result led to the expectation that SERS is observable with metallic nanoparticles. There are some different hypotheses established for the years to discuss the cause of SERS by LSPR. It is basically agreed in these days that the main cause of the enhancement is caused by enhanced electromagnetic field at the surface of the metal substrate. The second mechanism is considered with the "chemical enhancement". This explains that the incident light causes charge transfer with metallic materials, resulting to the enhancement of the resonance. This chemical enhancement is highly depends on the configuration of metallic surface and the nature of the sample molecules. Signal enhancement in SERS allows us the measurement even with low sample concentration, low power irradiance, and low measurement time (it was reported by Fang et al. that the average enhancement factor could reach up to 10^7 [12]). SERS has been applied to detect various inorganic/organic chemicals and biological materials [13-15].

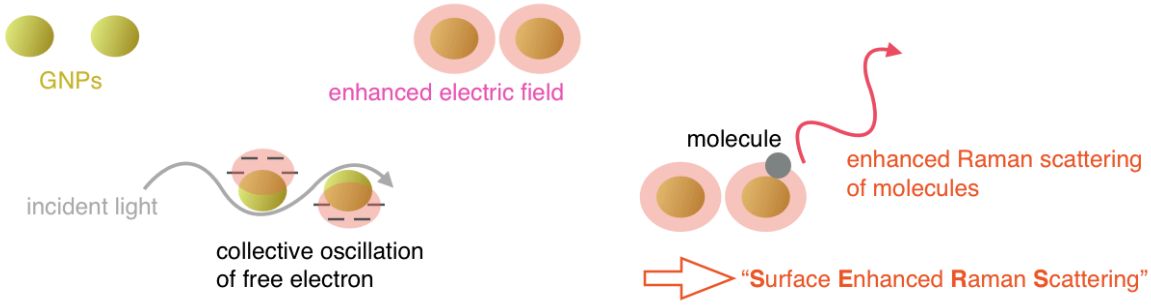

Fig. 6-2. The schematic of enhanced Raman scattering of a molecule adsorbed on light-excited gold NPs.

SERS measurement for biological cells

SERS measurements using metallic nanostructures have ever applied to investigate intracellular materials. The detection of SERS signals of native chemicals inside cells was reported in 2002, using gold nanoparticles (NPs) [16]. The introduction of NPs into cells was achieved by cellular uptakes called “endocytosis” [17]. When cells are incubated in medium with NPs, they introduced NPs inside them through receptor-mediated endocytosis first and trapped them in small vesicles known as “endosomes”. The introduction efficiency of NPs into cells depends on their size and shape [18].

These endosomes fuse with lysosomes and then those trapped NPs are transported to the cell periphery for excretion. Therefore, NPs introduced in cells through endocytosis exist only in vesicles inside cells, which indicates that only SRES of molecules inside vesicles can be detected with those NPs. It was naturally expected to detect SERS from other than inside vesicles in cells for biological and medical investigation. This passive uptake is easy for NPs to escape from the endosomal/lysosomal pathway. Although the optimal size of gold NPs for SERS measurement is in the range between 20 to 60 nm as reported by A. Wei et al., materials with those sizes are difficult to escape from the endosomal/lysosomal course [19, 20].

In order to overcome the problem mentioned above, some techniques have been reported. In 2007, A. Shamsaie et al. reported a method which fabricates gold NPs through cellular enzyme reduction [20]. They succeeded detecting SERS spectra from outside vesicles in HeLa cells, and showed the spectra which property was different from those gotten with gold NPs introduced by endocytosis. In 2009, W. Xie et al. reported the detection of SERS from nucleus in HeLa cells by tagging some peptides to gold NPs which makes them enter inside nucleus [21]. The functionalized gold NPs were firstly introduced into cells through cellular passive uptake, and tagged peptide worked to introduce NPs into nucleus. And E. A. Vitol et al. reported the use of glass nano-pipette on which gold NPs were attached, and showed detection of SERS from desired position in cells by inserting it into cells mechanically [22]. Up to here, some researches which reported SERS detection from outside vesicles were shown.

Expected more usability, I propose a technique to prepare gold NPs inside cells with more space selectivity, non-label, and non-destructive way. I adopted the use of laser-induced photoreduction to fabricate gold NPs at desired position inside biological cells.

6.2 Fundamentals of photoreduction

Aiming high spatial selectivity, non-label and non-destructive way, I proposed to fabricate gold NPs inside cells using laser-induced photoreduction. In this concept, the gold ions introduced in cells are reduced only at the laser-focused spots and high spatial selectivity for detecting SERS is expected. Here I'd like to show some fundamentals about photoreduction. In photoreduction process, the zero-valent metals (M^0) are formed from a metal source such as metal salt or ions. This photoreduction is achieved either with "direct photoreduction" way or "photosensitization" way. The latter method realizes fabrication of metal NPs using reducing agents such as excited molecules, radicals, and it is denoted as "indirect photoreduction" way against direct photoreduction in this dissertation. The first discovery of photoreduction of metals was done by H. H. Schulze in the 18th century from the blackening of silver salts after the irradiation of light [23]. The main advantages of photoreduction method are clean process, high spatial resolution defined by the diffraction limit of light source like laser and flexibility for mediums; solution, polymer, glasses, biological cells, etc [24-26].

Direct photoreduction has received attentions because it does not need from reducing agents. By direct photoreduction, M^0 forms through the direct excitation of metal source. The irradiation of UV pulsed light to gold ions ($AuCl_4^-$) in an aqueous solution is known to produce gold NPs. Although the high absorbance of $AuCl_4^-$ for UV wavelength range is known, its precise reduction mechanism is still not clear [27,28]. Interestingly, Eustis et al. found that gold NPs are not fabricated with photoreduction from $AuBr^{4-}$ [29]. The steric effect of bromide ions seems to prevent the formation of the Au^0-Au^0 bond needed in the electron transfer process. It is concluded that disproportionation of the chloroauric complexes is needed to generate gold atoms and chloride ions. Because this direct

photoreduction seems to need high photon density in its reduction process, reduction of metal occurs in quite small area in the laser focus spot. Because of this advantage, some researchers succeeded in fabricating metal microstructures by scanning a focused laser spot [30,31].

Indirect photoreduction is conducted in the presence of reducing agents that induces the generation of intermediates by light exposure. Those intermediates reduce metal ions, basically by giving electrons to them. The advantage of indirect photoreduction is the flexibility of the excitation wavelength as well as the efficiency of metal NPs formation in contrast to the direct photoreduction. The wavelength for excitation depends on not the kind of the metal ions, but the reducing agents. Because of the use of reducing agents, what is more, CW light source also performs photoreduction of metal ions instead of pulsed laser in direct photoreduction. As examples of reagents, radicals and organic dyes are known. [32-34]. The stabilization of photoreduced NPs or nanostructures is also one of important factors in photoreduction to fabricate NPs with controlled size or configuration/distribution. A lot of stabilizing agents such as polymers, surfactants, and biological materials have been employed for now [35-38].

6.3 Fabrication of gold nanoparticles (GNPs) inside cells

In this section, the experimental results of photoreduction of gold ions inside cells are shown. The efficient and high-reproducible photoreduction of gold NPs has been expected for application to SERS measurement of intracellular chemicals. Indirect photoreduction method is known to have good advantages for efficiency and high-reproducibility for photoreduction process. To accomplish the indirect photoreduction in cells, reducing agents are required to exist inside cells. What I expected is that some native chemicals in cells work as reducing agents under light irradiation. In my understanding, there has been no report which showed photoreduction in cells, but some biological materials were found to work as reducing agents or stabilizer for indirect photoreduction. Cells are known to contain a various kinds of chemicals including proteins, DNA which were reported to work as stabilizers or reducing agents mentioned above. As trial, I conducted laser irradiation

into cells immersed with gold ion solution. The experimental protocol is as the following. i)HeLa cells were grown in cellular growing solution (Dulbecco Minimum Essential Media (DMEM) + 10% bovine serum) on glass bottom dishes with a diameter of 35 mm. ii)Cells were filled up with 2 mM $HAuCl_4$ diluted with phosphate buffered saline (PBS)(-) after washed out with PBS(-) twice. iii)After 20 minutes incubation in $HAuCl_4$ solution, 532 nm CW laser was focused to the cells through water immersion objective lens (laser power: 0.8 ~ 1.7 mW at the focus point, exposure time: 0.1 ~ 5 s, objective lens: 100x/1.0 (water immersion)).

The possibility of fabrication of gold NPs in cells was firstly shown by the appearance of black spots at the laser-irradiated points in cells in bright field image (see Fig. 6-3). Laser irradiation to gold ion solution outside cells was also conducted, but no contrast change was confirmed laser-irradiated points outside cells although the same laser irradiation to inside cells induced the contrast changes.

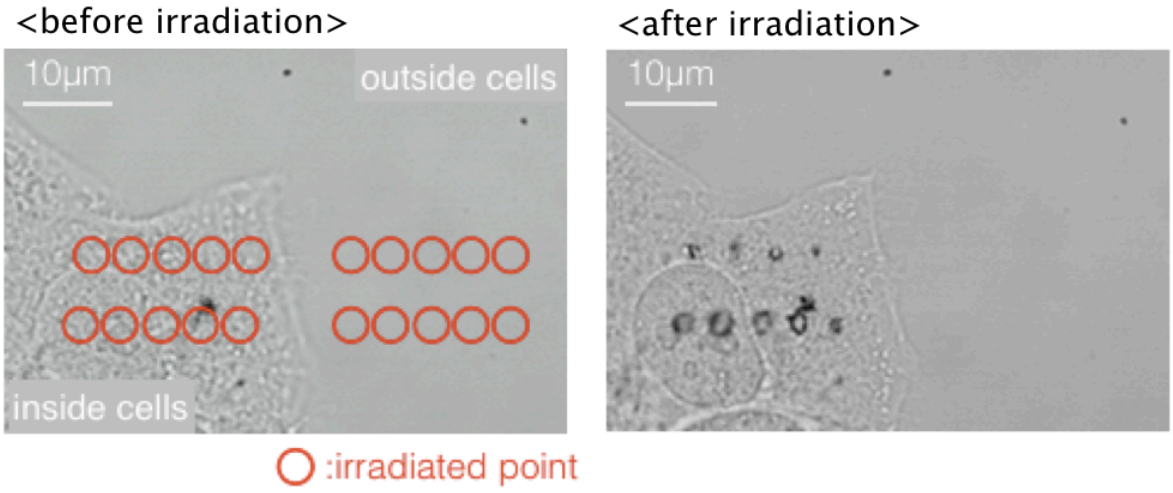

Fig. 6-3. Bright field images of inside and outside HeLa cells before and after 532 nm CW laser irradiation.

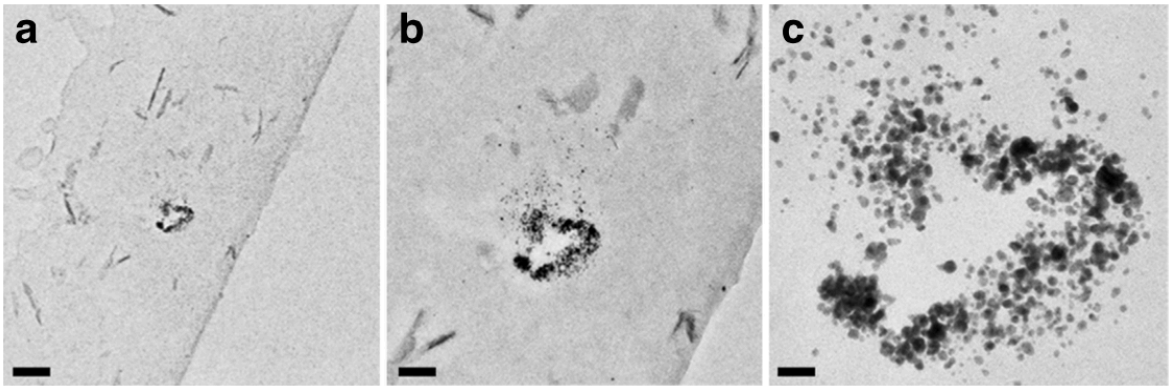

Fig. 6-4. Electron microscopy images of vertically sliced HeLa cells in which gold NPs were photoreduced. Scale bars for (a-c) are 310, 136, 39 nm, respectively. (Reprinted with permission from Macmillan Publishers Ltd.: Nature Communications, Smith, N. I. *et al.*, 5:5144 doi: 10.1038/ncomms6144 (2014), copyright 2014)

Those black points fabricated in cells were measured with transmission electron microscopy (TEM). Consequently, it was found that the gathering of 5 ~ 15 nm diameter of gold NPs were fabricated at the laser-irradiated point inside cells. Although a hollow at the irradiated position seemed to be generated by an explosion under photoreduction or in a process of sample preparation for TEM measurements, it was proven that gold NPs were fabricated inside cells with 532 nm CW laser-induced photoreduction. The size of the aggregation of gold NPs photoreduced in cells depended on the laser power and exposure time of laser irradiation as shown below. Absorption change due to the laser-irradiation to cells containing gold ions was measured by quantified from the contrast change in bright field images. Also, the absorption change measurement was conducted for the some control condition including i)with laser irradiation and without gold ions in cells ii)without laser irradiation and gold ions in cells, iii)with laser irradiation and gold ions outside cells, iv)with laser irradiation and without gold ions outside cells, v)with laser irradiation and without gold ions in cells. As results, almost no contrast change was confirmed in these conditions, suggesting that no gold NPs were fabricated in the condition other than with laser irradiation and

gold ions inside cells. Now, it can be assumed that gold NPs are photoreduced only inside cell but not outside cells even in gold ion solution.

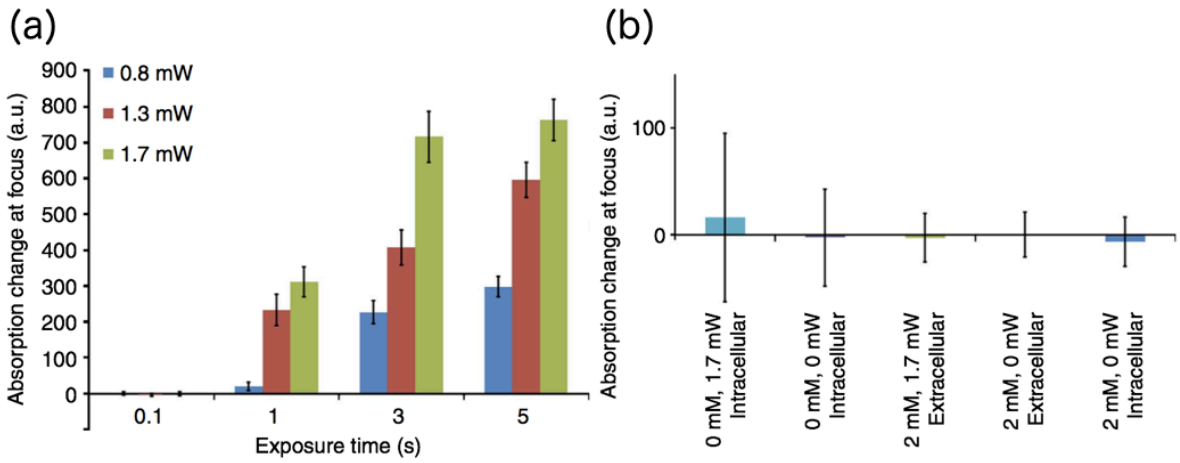

Fig. 6-5. (a)Absorption change due to laser-irradiation to cells (incubated in 2 mM $HAuCl_4$ with PBS (-)) with various laser power and exposure time, which was quantified from the contrast change in bright field images. (b)Absorption change in the control experiment, in which the experimental conditions are written. (Reprinted with permission from Macmillan Publishers Ltd.: Nature Communications, Smith, N. I. *et al.*, 5:5144 doi: 10.1038/ncomms6144 (2014), copyright 2014)

In fact, direct photoreduction of gold ions with visible CW laser has never reported for now in my understanding. Then one possibility came out that some materials or molecules worked as reducing agents activated by green laser irradiation, and gold NPs were fabricated in cells under indirect photoreduction process.

Also, the shape of those aggregation of gold NPs photoreduced in cells was controlled with micro-order scale by scanning the focused laser as shown below.

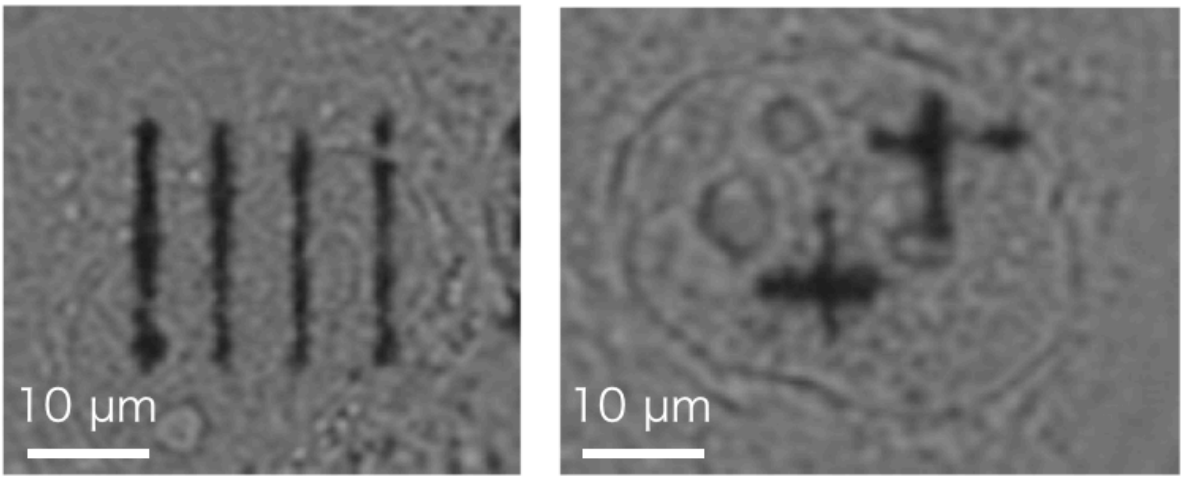

Fig. 6-6. Bright field images of gold structure inside cells, fabricated by scanning 532 nm CW laser.

6.4 Detection of SERS spectra

In this section, the result of SERS detection with gold NPs photoreduced in HeLa cells is shown. It was already shown that gold NPs was fabricated inside cells through laser-induced photoreduction technique. By 532 nm laser irradiation into gold ions-introduced HeLa cells, the aggregations of 5 ~ 15 nm gold NPs were fabricated in cells. From literatures, it is known that metal NPs of these sizes are well utilized to enhance Raman signals of native cellular chemicals by introduced into cell [20].

In advance of SERS measurement with photoreduced gold NPs, SERS measurement with commercial gold NPs was conducted to obtain experimental conditions for SERS detection. As explained in 3-1, cells introduce gold NPs in their growing-up medium by endocytosis [16]. In the case of HeLa cells, 50 nm gold NPs is known to be introduced into cells more than any other size of gold NPs by endocytosis [18]. And there are plenty of reports showing detection of SERS with 50 nm gold NPs introduced in biological cells via the cellular uptake [39-40]. Accordingly, 50 nm gold NPs was used to obtain the experimental condition for SERS detection in cells. Also, 20 nm gold NPs which size is closer to gold NPs fabricated in cells with photoreduction was tried. HeLa cells were cultured for 24 hours in DMEM containing 50 or 20 nm gold NPs at a concentration of 1.3

$\times 10^{10}$ particles/ml. Before Raman measurement, cells were washed out with PBS(-) twice and filled up with HEPES-buffered Tyrode's solution. SERS measurement was conducted with a commercial slit-scanning Raman microscope (**Raman11**, *Nanophoton*) at the excitation wavelength of 785 nm and a water immersion objective lens (100x/1.0, *Olympus*). In the Raman microscope, the excitation laser is line-shaped with a cylindrical lens and the two-dimensional image is acquired by scanning the line-shaped excitation light along one direction, resulting to the image acquisition with higher temporal resolution compared with the raster scan of point-focused light [41, 42]. Additionally, signals from defocused area in samples were filtered out by a confocal slit to obtain the confocality along the direction of scanning. As results, clear SERS spectra were obtained with both 50 nm and 20 nm gold NPs in HeLa cells with the laser power of 1.2 mW at the focused region, exposure time of 1 s/line, slit width of 80 μm. Although the signal/noise ratio of Raman spectra with 50 nm gold NPs is higher than that of 20 nm gold NPs, Raman peaks enhanced by the existence of 20 nm gold NPs were substantially distinguished. It can be concluded that SERS signals are detectable with the laser slit scanning of the optical system under the parameter written above, and SERS by 20 nm gold NPs was also detected, which showed the strong possibility of SERS detection with photoreduced gold NPs in cells.

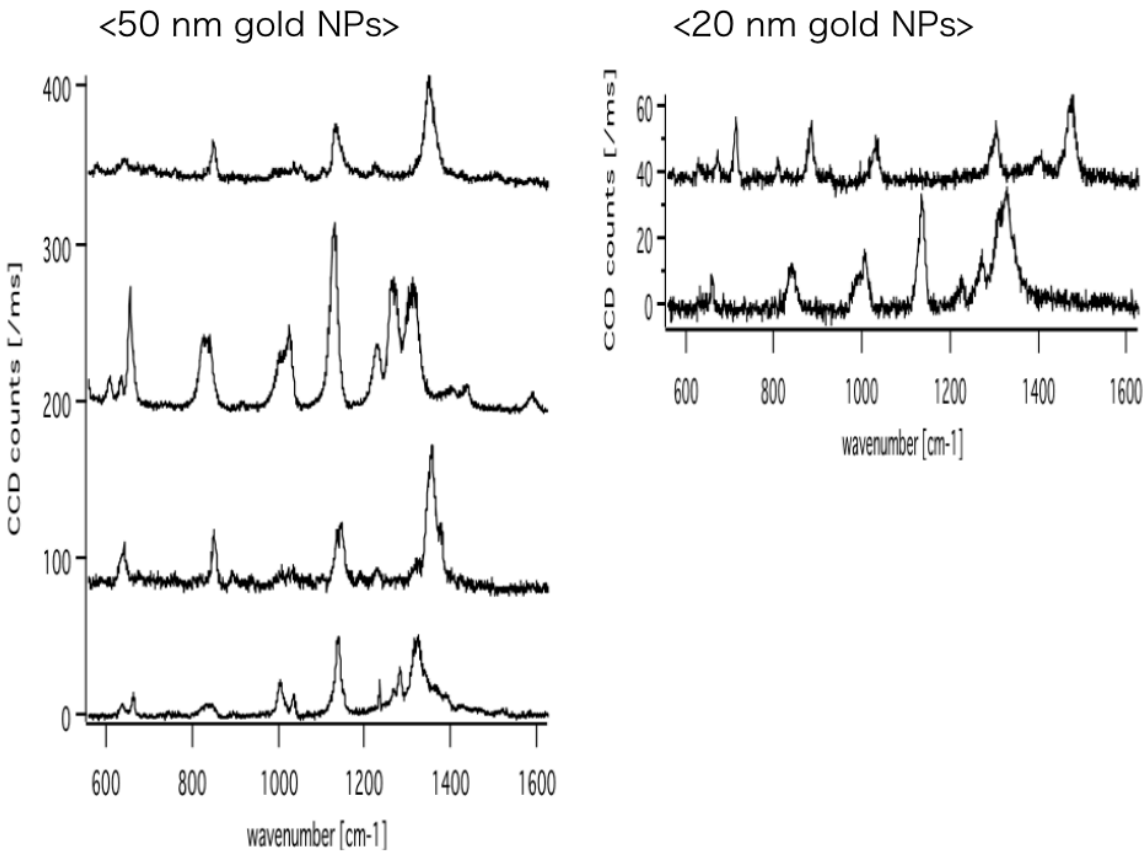

Fig. 6-7. SERS spectra gotten with commercial 50, 20 nm gold NPs introduced in HeLa cells by endocytosis.

Then I measured Raman spectra with gold NPs photoreduced in cells and investigated if enhanced Raman signals can be detected or not. For the investigation, various sizes of aggregations of gold NPs were fabricated inside cells by changing the laser irradiation parameters. For each laser irradiation parameter to photoreduced gold NPs, I investigated the probability of "fabrication of gold NPs" and "SERS detection with those fabricated NPs". As a tentative way, the fabrication of gold NPs was confirmed with the detection of luminescence from them excited with 532 nm excitation light [43]. Luminescence spectrum was also possible to be detected with the commercial Raman microscope as a function of Raman shift. As experimental protocol, i)HeLa cells were grown in DMEM with 10% bovine serum on glass bottom dishes with a diameter of 35 mm, ii)then they were incubated

in 2 mM $HAuCl_4$ diluted with PBS(-) after washed out with PBS(-) twice. iii)After 20 minutes incubation in $HAuCl_4$ solution, photoreduction of gold NPs in the cells was conducted with the irradiation of point-focused 532 nm CW laser (laser power: 0.8 ~ 1.7 mW at the focus spot, exposure time: 0.1 ~ 5 s, objective lens: 100x/1.0 (water immersion)). iv)Then Raman spectra in the area where laser irradiation for photoreduction was conducted were measured with line-shaped 785 nm CW laser (laser power: 1.2 mW at the focus spot, exposure time: 1 s/line, objective lens: 100x/1.0 (water immersion), slit width: 80 μm, center wavenumber: 1100 cm^{-1}). v)Finally, luminescence measurement was conducted to confirm the fabrication of gold NPs by photoreduction with line-shaped 532 nm CW laser (laser power: 2 mW, exposure time: 1 s/line, objective lens: 100x/1.0 (water immersion), slit width: 60 μm, center wavenumber: 1600 cm^{-1}). The laser irradiation for photoreduction of gold NPs was conducted to randomly chosen 30 points inside cells with various laser parameters (laser power: 0.8, 1.3, 1.7 mW at the laser-focused point, exposure time: 0.1, 1, 3, 5 s). Raman measurement for SERS detection was performed for each laser-irradiated points in cells. The result about the producibility of gold NPs through photoreduction and the detectability of SERS with them is organized in the table below. From the table, the number of luminescence detection, which can correspond to the generation of gold NPs, increases as laser power or exposure time for fabrication process increases. With more than 1.3 mW laser power and 3 s exposure time, luminescence was detected from more than 90 % of the points where laser was irradiated for photoreduction. However, the detectability of SERS signals with those gold NPs was not so high as the most one was almost 30 % even under 1.7 mW laser power and 5 s exposure time. Still, it was concluded that SERS could be detected with photoreduced gold NPs in HeLa cells.

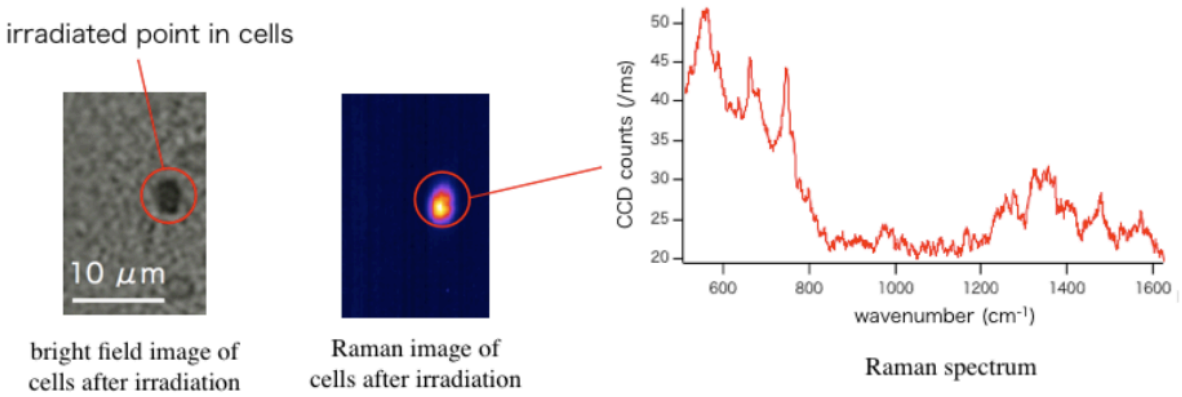

Fig. 6-8. Bright field image Raman image of photo-reduced gold NPs in HeLa cells and detected SERS spectra excited 785 nm wavelength laser.

exposure time \ laser power		0.8mW	1.3mW	1.7mW
0.1 s	SERS	0	0	0
	luminescence	0	0	1
	irradiated points	30	30	30
1 s	SERS	0	1	4
	luminescence	3	16	22
	irradiated points	30	30	30
3 s	SERS	1	6	10
	luminescence	12	24	29
	irradiated points	30	30	30
5 s	SERS	3	8	16
	luminescence	17	26	30
	irradiated points	30	30	30

Table 6-1. Table showing the number of laser irradiated point in HeLa cells and the number of point providing luminescence and SERS.

Next, all of SERS spectra gotten with photoreduced gold NPs are shown below. Each SERS spectrum was constructed by averaging all SERS spectra gotten with individual photoreduced gold NPs. Signal to noise ratio (SNR) of the spectra seems lower compared with those obtained with commercial gold NPs introduced in HeLa cells. In the TEM

images of fabricated gold NPs in cells shown in the previous chapter, laser-irradiated area showed some hollows in cells. Supposing that those hollows are generated by some factors in the photoreduction process such as explosions or heat generation, it may be possible that the destructive condition around fabricated gold NPs avoid me from obtaining high SNR. Or aggregation condition of NPs, which is one of important factors to realize SERS detection, could be not so optimized to provide high SNR.

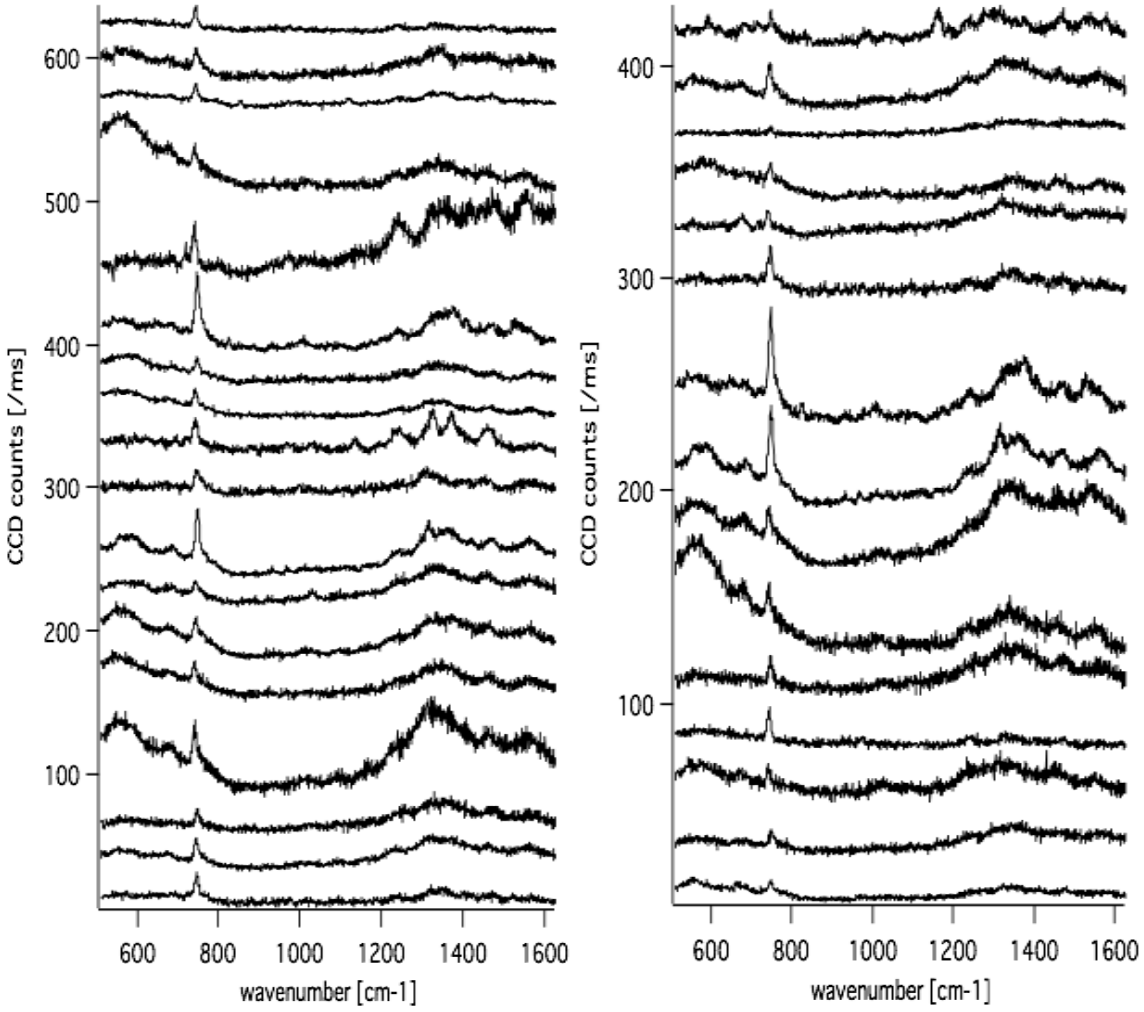

Fig. 6-9. SERS spectra gotten with gold NPs photoreduced in HeLa cells. One spectrum corresponds to average of all spectra from one fabricated gold NPs.

Interestingly, however, SERS spectra obtained with photoreduced gold NPs showed

exclusive Raman peaks at around 740 and 1350 cm^{-1}. This result does not correspond to the SERS spectra gotten with commercial gold NPs in cells and strongly suggests the existence of same chemicals around photoreduced gold NPs in cells. Accordingly, the chemicals can be assigned to the intracellular materials only existing outside vesicles, or materials generated in the process of photoreduction. Otherwise, it can be assumed that this materials helped photoreduction of gold NPs as sensitizers or stabilizers. This strongly suggested the possibility of investigation for photoreduction mechanism in my technique by identifying the materials. This is one of outlooks in this research.

Second outlook is to investigate the differences between SERS spectra obtained with NPs photoreduced in different position/organization in cells. Biological cells are constructed from various kinds of molecules or materials, and their composition or distribution are totally different between the location in cells such as cytoplasm, nucleus. For examples, cytoplasm contains more kinds of proteins than nucleus, and on the other hand, nucleus contains a wealth of amino acids which exist as a part of DNA. Some researchers succeeded getting Raman or SERS spectra from different location in cells (like inside vesicles, cytoplasm, nucleus, membrane), and showed the differences of them by assigning each Raman peaks or some analysis method [22, 45, 46]. As mentioned above, one of advantages of my photoreduction technique is to fabricate gold NPs at desired position in cells. Therefore, SERS spectra obtained with photoreduced NPs from different locations in cells is expected to reflect the differences of the molecular composition between locations. In this research, accordingly, distinguishing SERS spectra from cytoplasm and nucleus was tried. However, distinguishing them by assignment of each Raman peaks can be tentative because assignment process can depend on observers, and additionally the number of spectra is too many to assign all of them. Therefore, some other analysis methods were required in order to investigate them quantitatively and statistically such as principal component analysis (PCA).

References

[1] N. I. Smith, K. Mochizuki, H. Niioka, S. Ichikawa, N. Pavillon, A. J. Hobro, J. Ando, K.

Fujita, and Y. Kumagai, Nature Commun. 5:5144 (2014)

[2] C. V. Raman and K. S. Krishhan, *nature*, **121**, 501-502 (1928)

[3] 濱口宏夫、平川暁子　編「ラマン分光法」日本分光学会 (1988)

[4] T. R. Jensen, M. D. Malinsky, C. L. Haynes, R. P. V. Duyne, *J. Phys. Chem. B.*, **104**, 10549-10556 (2000)

[5] J. Z. Zhang and C. Noguez, *Plasmonics*, **3**, 127-150 (2008)

[6] S. L. and M. A. El-Sayed, *J. Phys. Chem. B*, **103**, 8410-8426 (1999)

[7] C. Noguez, *J. Phys. Chem. C*, **111**, 3806-3819 (2007)

[8] M. Fleischmann, P. J. Hendra, and A. J. McQuillan, *Chem. Phys. Lett.*, **26**, 163-166 (1974)

[9] D. L. Jeanmaire and R. P. V. Duyne, *J. Electroanal. Chem.*, **84**, 1-20 (1977)

[10] M. G. Albrecht, J. A. Creighton, *J. Am. Chem. Soc.*, **99**, 5215-5217 (1977)

[11] M. Moskovits, *J. Chem. Phys.*, **69**, 4159-4161 (1978)

[12] P.-P. Fang, J.-F. Li, Z.-L. Yang, L.-M. Li, B. Ren, Z.-Q. Tian, *J. Raman Spectrosc.*, **39**, 1679-1687 (2008)

[13] G. V. P. Kumar and J. Irudayaraj, *ChemPhysChem*, **10**, 2670-2673 (2009)

[14] J. F. Li, Y. F. Huang, Y. Ding, Z. L. Yang, S. B. Li, X. S. Zhou, F. R. Fan, W. Zhang, Z. Y. Zhou, D. Y. Wu, B. Ren, Z. L. Wang, Z. Q. Tian, *Nature*, **464**, 392-395 (2010)

[15] A. M. Schwartzberg, C. D. Grant, A. Wolcott, C. E. Tally, T. R. Huser, R. Bogomolni, and J. Z. Zhang, *J. Phys. Chem. B*, **108**, 19191-19197 (2004)

[16] K. Kneipp, A. S. Haka, H. Kneipp, K. Badizadegan, N. Yoshizawa, C. Boone, K. E. Shaferpeltier, J. T. Motz, R. R. Dasari, M. S. Feld, *Appl. Spectrosc.*, **56**, 150-154 (2002)

[17] B. D. Chithrani, J. Stewart, C. Allen, D. A. Jaffray, *Nanomedicine*, **5**, 118-127 (2009)

[18] B. D. Chirhrani, A. A. Ghazani, W. C. W. Chan, *Nano Lett.*, **6**, 4 (2006)

[19] A. Wei, B. Kim, B. Sadtler, S. L. Tripp, *ChemPhysChem*, **2**, 743-745 (2001)

[20] A. Shamsaie, M. Jonczyk, J. Sturgis, J. P. Robinson, J. Irudayaraj, *J. Biomed. Opt.*, **12**, 0205021-0205023 (2007)

[21] W. Xie, L. Wang, Y. Zhang, L. Su, A. Shen, J. Tan, J. Hu, *Bioconjugate Chem.*, **20**, 768-773 (2009)

[22] E. A. Bitol, Z. Orynbayeva, M. J. Bouchard, J. Azizkhan-Clifford, G. Friedman, Y. Gogotsi, *ACS Nano*, **3**, 3529-3536 (2009)

[23] M. Sakamoto, M. Fujistuka, T. Majima, *J. Photochem. Photobiol. C*, **10**, 33-56 (2009)

[24] M. Sakamoto, T. Tachikawa, M. Fujitsuka, and T. Majima, *Chem. Mater.*, **20**, 2060-2062 (2008)

[25] A. V. Kabashina and M. Meunier, *J. Appl. Phys.*, **94**, 7941-7943 (2003)

[26] T. Tanaka, A. Ishikawa, and S. Kawata, *Appl. Phys. Lett.*, **88**, 081107 (2006)

[27] J.-E. Park, M. Atobe, T. Fuchigami, *Electrochem. Acta*, **51**, 849-854 (2005)

[28] K. Kurihara, J. Kizling, P. Stenius, J. H. Fendler, *J. Am. Chem. Soc.*, **105**, 2574-2579 (1983)

[29] S. Eustis, M.-A. El-Sayed, *J. Phys. Chem. B.*, **110**, 14014-14019 (2006)

[30] K. Kaneko, H.-B. Sun, X.-M. Duan, and S. Kawata, *Appl Phys. Lett.*, **83**, 1426 (2003)

[31] P.-W. Wu, W. Cheng, I. B. Martini, B. Duan, B. J. Schwartz, E. Yablonovitch, *Adv. Mter.*, **12**, 1438 (2000)

[32] G. J. Kavarnos, "*Fundamentals of Photoinduced Electron Transfer*", Wiley-VCH (1993)

[33] K. L. McGilvray, M. R. Decan, D. Wang, J. C. Scaiano, *J. Am. Chem. Soc.*, **128**, 15980-15981 (2006)

[34] F. Stellacci, C. A. Bauer, T. Meyer-Friedrichsen, W. Wenseleers, V. Alain, S. M. Kuebler, S. J. K. Pond, Y. Zhang, S. R. Marder, J. W. Perry, *Adv. Mater.*, **14**, 194 (2002)

[35] A. Roucoux, J. Schulz, H. Patin, *Chem. Rev.*, **102**, 3757-3778 (2002)

[36] C. Burda, X. Chen, R. Narayanan, M. A. El-Sayed, *Chem. Rev.*, **105**, 1025-1102 (2005)

[37] L. Berti, A. Alessandrini, P. Facci, *J. Am. Chem. Soc.*, **127**, 11216 (2005)

[38] G. Wei, L. Wang, L. Sun, Y. Song, Y. Sun, C. Guo, T. Yang, and Z. Li, *J. Phys. Chem. C.*, **111**, 1976-1982 (2007)

[39] K. Fujita, S. Ishitobi, K. Hamada, N. I. Smith, A. Taguchi, Y. Inouye, S. Kawata, *J. Biomed. Opt.*, **14**, 0240381-0240387 (2009)

[40] A. Shamasie, J. Heim, A. A. Yanik, J. Irudayaraj, *Chem. Phys. Lett.*, **461**, 131-135

(2008)

[41] D. K. Veirs, J. W. Ager Ⅲ, E. T. Loucks, and G. M. Rosenblatt, *Appl. Opt.*, **29**, 4969-4980 (1990)

[42] K. Hamada, K. Fujita, M. Kobayashi, and S. Kawata, *Proc. SPIE*, 6443, 64430Z (2007)

[43] A. C. D. Luca, M. Mazilu, A. Riches, C. S. Herrington, K. Dholakia., *Anal. Chem.*, **82**, 738-745 (2006)

Conclusions

In my doctoral research, the stepwise multi-photon excitation was proposed to realize nonlinear fluorescence response by visible light excitation, which is equivalent to realize super-resolution microscopy with a conventional confocal laser-scanning microscope.

I utilized photoinduced charge separation (PCS) to realize stepwise two-photon excitation based on repetitive one-photon excitation. A fluorescent probe with two fluorophores and one electron acceptor was designed and synthesized according to my concept of the stepwise two-photon excitation, and named nitro-bisBODIPY. The first incident photon absorbed by this probe induces a charge-separated state between one of the donors and an acceptor, and then the second photon absorbed by this probe can be used for fluorescence excitation of the other donor. The 2nd order nonlinear fluorescence response of nitro-bisBODIPY was experimentally detected by exciting the probe with a 488 nm CW laser light. Fluorescence imaging of HeLa cells stained with nitro-bisBODIPY was conducted with the same optical setup to evaluate the practical utility of nitro-bisBODIPY, and the improvement in image contrast and resolution was confirmed.

A photophysical model of the stepwise two-photon excitation via PCS was investigated by building the energy model of nitro-bisBODIPY. The five-level energy diagram of nitro-bisBODIPY including charge-separated states was proposed. To determine the parameters for electronic transition in the model, transient absorption spectra of nitro-bisBODIPY was measured. The results provided the rate constants of the generation and decay of the charge-separated state in the probe. Using the model and parameters, the simulation of excitation-emission response of the probe was conducted. As results, the good consistency of the simulation and experimental results showed that the photophysical mechanism of the nonlinear optical response by nitro-bisBODIPY was based on the proposed energy diagram.

I also proposed a concept to achieve stepwise three-photon absorption using spirocyclic compounds. In this scheme, stepwise three-photon excitation can be realized via two-photon absorption to induce spirocycle opening and subsequent one-photon absorption under visible-wavelength pulsed excitation to excite the fluorescence. Experimentally,

fluorescence response of three kinds of spirocyclic compounds (HySOx, MMSiR, RSA) under the visible wavelength pulsed excitation were measured, which absorption peaks for fluorescence excitation and lifetimes of spirocycle opening were different. A 3rd order nonlinear fluorescence response was detected with MMSiR under 610 nm pulsed excitation. Theses results show that the concept can be applied to super-resolution fluorescence microscopy, where a 1.7 fold improvement of spatial resolution is expected compared to conventional confocal microscopy.

I also investigated the use of near-field light on metallic nanostructure to image intracellular molecules and developed a probe to detect SERS spectra inside cells with high spatial selectivity. The probe was composed of gold NPs and fabricated at desired positions in cells using laser-induced photoreduction. Gold ions introduced into the cell bodies were photoreduced to aggregations of gold NPs only at the laser-focused points, which were confirmed by using bright field images and transmission electron microscopy. The size of the aggregation was controlled by changing the intensity and exposure time of the excitation. Finally I confirmed the detection of SERS spectra from the probes photoreduced inside cells.

Appendices

Synthesis

Nitro-bisBODIPY (STEP1)

2-Nitro terephtalic acid methyl ester (2.39 g, 10 mmol) was dissolved in dry toluene (25 ml) and stirred several minutes under Ar atmosphere. The reaction mixture was cooled down to −70 ˚C by acetone/dry ice bath. DIBALH (22 ml, 17% in toluene, 1 M) was added with a syringe over 1 h to that the temperature did not exceed −65 ˚C. The white slurry was stirred for 4 h under −40 ˚C. MeOH (10 ml) was added slowly to ensure the reaction temperature did not exceed −40 ˚C. Finally, the reaction mixture was poured into a mixture of ice (100 ml) and hydrochloric acid (2 N, 100 ml). The aqueous solution was extracted with CH_2Cl_2, and the organic layer was dried over Na2SO4 and evaporated to yield crude material. Recrystalization from heptane gave terephthalaldehyde as yellow solid (1.5 g, 80%).

1H NMR (400 MHz, CDCl3): δ 8.09 (d, 1H, J = 7.2 Hz), 8.26 (d, 1H, J = 7.2 Hz), 8.60 (s, 1H), 10.16 (s, 1H), 10.47 (s, 1H). 13C NMR (100 MHz, CDCl3): δ 124.4, 124.5, 130.3, 133.8, 134.5, 139.1, 187.1, 188.8. MS (ESI+): m/z calcd for [M+H] + 180.0, Found: 180.1.

Nitro-bisBODIPY (STEP2)

2-Nitro-terephthalaldehyde (360 mg, 2 mmol) and 2,4-dimethylpyrrole (760 mg, 8 mmol) were dissolved in 100 mL of absolute CH_2Cl_2 under Ar atmosphere. One drop of TFA was added under 0 ˚C, and the solution was stirred at room temperature overnight. When TLC monitoring (silica gel, CH_2Cl_2) showed complete consumption of the terephthalaldehyde, a solution of DDQ (940 mg, 4 mmol) in 1:1 THF/CH_2Cl_2 was added and stirring was continued for 1 h. To this solution, 3 mL DIPEA was added and stirring was continued for 40 min. Then, 3 mL BF_2-Et_2O was added, and the solution was stirred at room temperature for 1 h. The reaction mixture was filtered first by removing the solid in the mixture. Then, the solution after filtering washed with 2 N NaOH aqueous solution and water, dried over Na_2SO_4, filtered and evaporated. The residue was purified by flash

chromatography (silica gel, CH_2Cl_2) to give dark-green solid (0.14 g, 10%).

1H NMR (400 MHz, CDCl3): δ 1.43 (s, 12H), 2.28 (s, 12H), 5.83 (s, 2H), 5.88 (s, 2H), 7.19 (d, 1H, J = 7.5 Hz), 7.54 (d, 1H, J = 7.5 Hz), 8.04 (s, 1H). 13C NMR (100 MHz, CDCl3): δ 15.5, 16.0, 16.6, 119.9, 120.3, 126.4, 132.5, 132.9, 133.2, 135.0, 136.4, 138.5, 139.0, 140.1, 150.1, 152.3, 152.7. MS (ESI+): m/z calcd for [M+H]+ 616.26, Found: 616.28. Anal. Calcd for C19H19BF2N2: C, 57.94; H, 4.82; N, 10.32. Found: C, 57.87; H, 4.85; N, 9.93.

Nitro-monoBODIPY

2-Nitrobenzaldehyde (151 mg, 1 mmol) and 2,4-dimethylpyrrole (190 mg, 2 mmol) were dissolved in 50 mL of absolute CH_2Cl_2 under Ar atmosphere. One drop of TFA was added, and the solution was stirred at room temperature for 7–8 h. When the TLC monitoring (silica gel, CH_2Cl_2) showed complete consumption of the 2-nitrobenzaldehyde, a solution of DDQ (227 mg, 1 mmol) in 1:1 THF/CH_2Cl_2 was added and stirring was continued for 30 min. To this solution, 1.5 mL dry DIPEA was added and stirring was continued for 20 min. Then, 1.5 mL BF_3 in Et_2O was added, and the mixture solution was stirred at room temperature for 30 min. The reaction mixture was washed with water, dried over Na_2SO_4, filtered and evaporated. The residue was purified by flash chromatography (silica gel, CH_2Cl2_2) to give dark-green solid (0.21 g, 57%).

1H NMR (400 MHz, CDCl3): δ 1.36 (s, 6H), 2.56 (s, 6H), 5.99 (s, 2H), 7.50 (d, 1H, J = 7.5 Hz), 7.56 (t, 1H, J = 7.5 Hz), 7.82(t, 1H, J = 7.5 Hz), 8.22 (d, 1H, J = 7.5 Hz). MS (ESI+): m/z calcd for [M+H]+ 370.15, Found: 370.15. Anal. Calcd for C19H18BF2N3O2: C, 61.81; H, 4.91; N, 11.38. Found: C, 61.87; H, 5.13; N, 11.41.

bisBODIPY

Terephthalaldehyde (268 mg, 2 mmol) and 2,4-dimethylpyrrole (760 mg, 8 mmol) were dissolved in 100 mL of absolute CH_2Cl_2 under Ar atmosphere. One drop of TFA was added, and the solution was stirred at room temperature overnight. When TLC monitoring (silica gel, CH_2Cl_2) showed complete consumption of the terephthalaldehyde, a solution of DDQ

(940 mg, 4 mmol) in 1:1 THF/CH_2Cl_2 was added and stirring was continued for 1 h. To this solution, 3.5 mL DIPEA was added and stirring was continued for 40 min. Then, 3.5 mL BF_3-Et_2O was added, and the solution was stirred at room temperature for 1 h. The reaction mixture was filtered first, then the clear solution was washed with water, dried over Na_2SO_4, filtered and evaporated. The residue was purified by flash chromatography (silica gel, CH_2Cl_2) to give red solid (0.25 g, 22%).

1H NMR (400 MHz, CDCl3): δ 1.49 (s, 6H), 2.53 (s, 6H), 5.95 (s, 4H), 7.48 (s, 4H). MS (ESI+): m/z calcd for M+ 570.27, Found: 570.36. Anal. Calcd for C32H32B2F4N4 : C,64.76; H, 5.49; N, 9.34. Found: C, 64.67; H, 5.37; N, 9.31.

Publications

Original papers

[1] Kentaro Mochizuki, Lanting Shi, Shin Mizukami, Masahito Yamanaka, Mamoru Tanabe, Wei-Tao Gong, Almar F Palonpon, Shogo Kawano, Satoshi Kawata, Kazuya Kikuchi, and Katsumasa Fujita, "Nonlinear fluorescence imaging by photoinduced charge separation", *Jpn. J. Appl. Phys.* (Accepted)

[2] Masahito Yamanaka, Kenta Saito, Nicholas I. Smith, Yoshiyuki Arai, Kumiko Uegaki, Yasuo Yonemaru, Kentaro Mochizuki, Satoshi Kawata, Takeharu Nagai, and Katsumasa Fujita, "Visible-wavelength two-photon excitation microscopy for fluorescent protein imaging", *J. Biom. Opt.* (Under revision)

[3] Nicholas I. Smith, Kentaro Mochizuki, Hirohiko Niioka, Satoshi Ichikawa, Nicolas Pavillon, Alison J. Hobro, Jun Ando, Katsumasa Fujita, and Yutaro Kumagai, "Laser-targeted photofabrication of gold nanoparticles inside cells", *Nat. Comm.*, **5**, 5144 (2014)

International conferences

[1] Kentaro Mochizuki, Lanting Shi, Shin Mizukami, Masahito Yamanaka, Wei-Tao Gong, Shogo Kawano, Satoshi Kawata, Kazuya Kikuchi, Katsumasa Fujita, “Developing Nonlinear Reaction Probe to Improve the Spatial Resolution of Fluorescence Microscopy” International Symposium on Atomically Controlled Fabrication Technology, February 2014

Domestic conferences

[1] Kentaro Mochizuki, Nicholas I. Simith, "Fabrication of gold nanoparticles in cells by laser-induced photoreduction" The 49th Annual Meeting of the Biophysical Society of Japan, September 2011

[2] Kentaro Mochizuki, Lanting Shi, Shin Mizukami, Masahito Yamanaka, Mamoru Tanabe, Wei-Tao Gong, Shogo Kawano, Nicholas I. Simith, Satoshi Kawata, Kazuya Kikuchi, Katsumasa Fujita, "Development of a Fluorescent Probe Providing Nonlinear Response through Intramolecular Electron Transfer" The Japan Society of Applied Physics 75th Autumn meeting, September 2014

[3] Kentaro Mochizuki, Lanting Shi, Shin Mizukami, Masahito Yamanaka, Mamoru Tanabe, Wei-Tao Gong, Shogo Kawano, Satoshi Kawata, Kazuya Kikuchi, Katsumasa Fujita, "Nonlinear fluorescence probe using photoinduced charge separation", Optics & Photonics Japan 2014, November 2014

Acknowledgement

I appreciate to all people who have supported my research life.

Prof. Satoshi Kawata (Dept. of Applied Physics, Osaka Univ.) for motivating me to join in scientific research life and giving me tremendous supports. I learned from him not only how to research but also what is science.

Associate Prof. Katsumasa Fujita (Dept. of Applied Physics, Osaka Univ.) for his hearty education and all supports for my research. My research was advanced with his advices, comments, helps.

Associate Prof. Nicholas I. Smith (Immunology Frontier Research Center (IFReC), Osaka Univ.) for his many comments, advice and helps on my research.

Prof. Yasushi Inouye (Frontier Biosciences, Osaka Univ.) for his advice on my research.

Prof. Eiichi Tamiya (Dept. of Applied Physics, Osaka Univ.) and Prof. Yoshimasa Kawata (Dept. of Mechanical Engineering, Shizuoka Univ.) for giving me a lot of comments and suggestions on my dissertation.

Prof. Kazuya Kikuchi and Associated Prof. Shin Mizukami (Div. of Advanced Science and Biotechnology, Osaka Univ.) for helping to develop the nonlinear fluorescent probes.

Assistant Prof. Masahito Yamanaka (Dept. Quantum Engineering, Nagoya Univ.) for his great helps and advice for my research.

Yasuo Yonemaru (Dept. of Applied Physics. Osaka Univ.) for working together during my doctoral course and giving me a lot of helps, comments, suggestions.

Dr. Shogo Kawano (Nanophoton corp.), Dr. Jun Ando, Dr. Almar Palonpon, Dr. Yasuaki Kumamoto, Dr. Lanting Shi (Dept. of Applied Physics, Osaka Univ.) for their daily support for my research.

Toshihiro Mino, Shota Ushiba, Maouli Imad, and Kozue Watanabe (Dept. of Applied Physics, Osaka Univ.) for all helps in my research life.

And all members in my laboratory for their helps in my research life.